Protein encapsulation in functionalized sol-gel silica: influence of organosilanes and main silica precursors

Rémi G. Tilkin[*a,b], Julien G. Mahy[c], Nicolas Régibeau[a,b], Romain Vandeberg[b], Ana P. F. Monteiro[a,b], Christian Grandfils[b], Stéphanie D. Lambert[a]*

[a] Department of Chemical Engineering – Nanomaterials, Catalysis and Electrochemistry (NCE), University of Liège, Allée du Six Août 11, 4000 Liège, Belgium

[b] Interfaculty Research Center of Biomaterials (CEIB), University of Liège, Allée du Six Août 11, 4000 Liège, Belgium

[c] Institute of Condensed Matter and Nanosciences (IMCN), Université catholique de Louvain, Place Louis Pasteur 1, 1348, Louvain-la-Neuve, Belgium

Corresponding author: Rémi G. Tilkin; email: rtilkin@uliege.be ; address: Allée du Six Août 11, 4000 Liège, Belgium

ABSTRACT

Over the last few years, bone repair has increasingly gained in importance. In recent years, considerable attention has been given to the administration of therapeutic biomolecules to promote tissue regeneration. The aim of this work is the study of the influence of functional groups present at the surface of silica pores on the release kinetics of a model protein (*i.e*. Soybean Trypsin Inhibitor, STI). The carried protein was examined via: i) the impregnation of silica gels in the protein solution after the silica gel drying and/or calcination (*i.e*. impregnation method), and ii) the direct incorporation of the protein during the silica gel synthesis (*i.e*. *in situ* method). Surface chemistry and textural properties were tuned using different organosilanes (*i.e*. functionalized silanes containing amine, ethylene diamine, or phenyl groups) and different main silica precursors (*i.e*. containing methoxy or ethoxy groups). These physicochemical modifications were shown to deeply affect the immobilization and release kinetic of STI. In particular, for both encapsulation methods, phenyl-modified samples presented a high amount of encapsulated STI accompanied by a very low release of STI over the 85 days period. The other functional groups gave rise to a lower encapsulation yield. Regarding the protein release profiles, a fast release of STI was observed for the samples prepared via the impregnation method, which showed a burst effect followed by a sustained release until day 30. On the opposite, the *in situ* method allowed a better control of the release rate of this protein over the first 24 h followed by a sustained released up to 85 days.

Keywords: biomaterials, bone reconstruction, protein encapsulation, silica gel, sol-gel process, organosilane.

1. INTRODUCTION

Over the last decades, bone repair has increasingly gained in importance due to the expanding market of surgical procedure involving bone grafting or bone graft substitutes (*i.e.* over 4 million surgical procedures performed every year worldwide) and the ageing population (*i.e.* almost doubling of the population over 65 years in 2050) [1–3]. Several methods have been proposed to recover the complete structure and function of the native bone. In recent years, considerable attention has been given to the administration of therapeutic biomolecules to improve tissue regeneration [4,5].

In the case of bone reconstruction, several biomolecules have been considered. Among these, bone morphogenetic proteins (BMP), a family of cytokines, have been widely investigated [6–8]. Indeed, in bone tissue, BMPs regulate the bone formation by controlling the cell adhesion, proliferation, differentiation, and apoptosis. In particular, studies have demonstrated that BMP-2 could recruit osteogenic progenitor cells and stimulate the bone differentiation of stem cells, hence promoting the fracture repair [9–11]. In this context, BMP-2 and BMP-7 have been approved by the US Food and Drug Administration for the treatment of bone fractures [6,12]. Nevertheless, BMPs cannot be directly injected into the fracture site because an excessively high dose of growth factors would lead to an undesirable growth of tumors or neovascularization of non-targeted tissues [13]. Careful attention must therefore be paid to the release kinetics of BMPs in order to achieve a safe and efficient bone reconstruction process.

Several delivery system have already been studied for the sustained delivery of BMP [14–16]. In particular, silica gels appear as promising matrices for the controlled release of different biomolecules in tissue engineering [17–22]. Silica gels consist of an interconnected structure of silicon atoms forming an amorphous porous material [23–26]. They exhibit a high porosity and a large specific surface area, allowing the adsorption of a large amount of biomolecules [27].

Moreover, these gels can be synthesized in soft conditions (*e.g.* via sol-gel processing) that are not detrimental for the activity of these biomolecules [23–26]. Furthermore, silica gels can be further processed in a large range of forms such as monoliths, films, and particles [17,23,28]. In addition to its biocompatibility (*i.e.* resorbable and non-toxic), silica can protect enzymes against physicochemical stresses, maintaining their structural integrity and biological activity [19,23,27,29]. Another attractive feature of this material is the possibility to tune the interaction between the protein and its substrate via control of the morphology and the surface composition of the pores. On the one hand, the pore morphology regulates the diffusion of the protein inside the silica pores and the subsequent release process [17,26,30]. The silica porosity can be modified by modulating the synthesis conditions (*e.g.* pH, solvent, processing conditions). On the other hand, the surface chemistry of the pores can be tuned using functional groups exhibiting different charges or hydrophilic/hydrophobic properties that modulate the interaction between the pores and the protein (*i.e.* electrostatic forces, hydrogen bonding, van der Waals forces, covalent interactions) [28,30–32]. The textural properties and surface chemistry of the silica gels should be specifically adapted to each protein in order to match its characteristics, in terms of surface charge distribution, size, secondary and tertiary structures, hydrophobicity, and surface reactivity.

Table 1. Properties of STI and BMP-2

Properties	**STI**	**BMP-2**
Molecular weight (g/mol)	21,000 [23,33]	26,000 [23]
Size (nm)	4.5 x 4.2 x 4 [34]	7 x 3.5 x 3 [35]
Point of zero charge (*pH* unit)	4.5 [36]	4.8-5.1 [37]

In this study, Soybean Trypsin Inhibitor (STI) has been selected as a model protein because of its similarities with the BMPs in term of size, molecular weight, point of zero charge, hydrophobic properties, and release kinetics (Table 1) [23,38,39]. Moreover, this protein has been previously

used to model BMP release from porous silica [23,33,39,40]. The encapsulation of BMP and STI inside silica gels and their release from this matrix have already been studied. BMP and STI have been incorporated though the impregnation of previously synthesized gels (*i.e.* impregnation method) [4,5,40–46] and the direct incorporation of these proteins during the gel formation (*i.e. in situ* method) [13,23,33,40,47,48]. The results have shown a STI or BMP loading in the range 0.2-4 $mg_{protein}/g_{silica}$ and a sustained release from 24 h up to 9 weeks. Nevertheless, fast release over the first 24 h, referred to as burst release, were frequently observed [23,43–45,48] and some samples exhibited a high protein retention [41,42,46,48]. Regarding the protein activity, moderate loss of activity has been disclosed, although very few studies have assessed this important parameter [23,40,43]. It is worth noting that the surface chemistry and the textural properties of silica considerably influence the protein encapsulation and release by regulating their diffusion inside the pores via their interaction with the pore walls. They also influence the protein activity through the modulation of the interaction with functional groups present at the pore surface or through physical restriction of the protein conformation [28,30]. The understanding of the influence of textural properties (*e.g.* pore size, specific surface area) and surface chemistry (*e.g.* addition of specific functional groups) on the STI encapsulation and release is therefore relevant. Only two studies have already been carried out on the impact of surface modification on STI and BMP-2 encapsulation, release, and activity. Ehlert *et al*. have encapsulated BMP-2 in 3-aminopropyl-modified silica using an impregnation technique [46]. The results have shown a significant increase in BMP-2 loading for the 3-aminopropyl-modified silica compared to the unmodified silica as well as a high BMP-2 retention, as about 5 % of the originally bound BMP-2 was released. In another study, our group has studied the influence of other amine groups (*i.e.* ethylene diamine groups) on the encapsulation and release of STI via an impregnation technique [40]. In this study, silica synthesized via a co-condensation method was used after drying (*i.e.* presence of ethylene diamine

groups) or calcination (*i.e.* bare silica). The results have shown that similar STI loading were obtained for the ethylene diamine-modified samples compared to the unmodified ones. When incubated in physiological conditions, a fast release of STI was observed over the first 24 h, followed by a plateau for the calcined samples or by a sustained release up to 85 days for the dried sample. Moreover, the modified sample exhibited a residual activity (30 %) after 4 weeks of incubation while a total loss of activity was observed for the unmodified ones. As can be seen from these studies, only hydrophilic groups (*i.e.* amine groups) were grafted onto the silica surface. Moreover, the impregnation method was the only one assessed while it has been shown that the nature of the encapsulation technique greatly influences the STI release and activity [40]. Therefore, these previous works should be expanded via the use of hydrophobic groups and via the comparison of different encapsulation methods (impregnation and *in situ*).

Based on this rational, hydrophilic (*i.e.* organosilanes containing ethylene diamine or 3-aminopropyl groups) and hydrophobic groups (*i.e.* organosilanes containing phenyl group) were grafted onto the silica surface. Surface chemistry and textural properties were further controlled via the use of different main silica precursors (*i.e.* tetraethyl orthosilicate and tetramethyl orthosilicate). Moreover, the protein was encapsulated via two methods: impregnation and *in situ* method. The influence of the organosilanes and the main silica precursor were determined via infrared spectroscopy (FTIR) to study the chemical composition, thermogravimetric analysis (TGA) to determine the organic content, nitrogen adsorption-desorption measurements and mercury porosimetry to assess the textural properties, and by the method of equilibrium *pH* at high loading to determine the point of zero charge (PZC). The release kinetics of the protein *in vitro* as well as the inhibitory activity after release were also determined over a period of 12 weeks.

2. MATERIALS AND METHODS

2.1. Materials

In this section, the activity of the proteins is expressed in N_α-Benzoyl-L-arginine ethyl ester hydrochloride (BAEE) units. In this context, one BAEE unit yields a difference of absorbance at 253 nm (ΔA_{253}) of 0.001/min with BAEE as substrate at *pH* = 7.6 at 25 °C.

Tetraethyl orthosilicate (TEOS, $Si(OC_2H_5)_4$), ammonium hydroxide solution (NH_3, 28-30 %), 3-(2-aminoethylamino)propyltrimethoxysilane (EDAS, $(CH_3O)_3Si(CH_2)_3NHCH_2CH_2NH_2$ (97 %)), monobasic potassium phosphate (KH_2PO_4), sodium chloride (NaCl), potassium chloride (KCl), and Trypsin from bovine pancreas (Type I, 10,000 BAEE units/mg) were purchased from Sigma-Aldrich; absolute ethanol (C_2H_5OH), hydrochloric acid (HCl (37 %)), (3-aminopropyl)trimethoxysilane (APTMS, $(CH_3O)_3Si(CH_2)_3NH_2$), and sodium hydroxide (NaOH) from Merck; tetramethyl orthosilicate (TMOS, $Si(OCH_3)_4$), dibasic sodium phosphate (Na_2HPO_4), monobasic sodium phosphate (NaH_2PO_4), and N_α-benzoyl-L-arginine ethyl ester hydrochloride (BAEE, $C_{15}H_{22}N_4O_3 \cdot HCl$) from Acros Organics; Soybean Trypsin Inhibitor STI (≥ 7000 BAEE U/mg) from Carl Roth; phenyltrimethoxysilane (PTMS, $(CH_3O)_3SiC_6H_5$, 97 %) from Alfa Aesar. Unless indicated otherwise, all these chemicals were ≥ 99 % pure and were used without further purification. Phosphate Buffer Saline (PBS) solution was prepared using 1.4 mM KH_2PO_4, 10 mM Na_2HPO_4, 137 mM NaCl and 2.7 mM KCl and was adjusted to pH = 7.4 using 0.1 M HCl or 0.1 M NaOH.

2.2. Sample preparation

Two processes were used in this study for the encapsulation of STI in silica gels: an impregnation method and an in situ method. EDAS, APTMS, and PTMS were used as organosilanes, and TEOS and TMOS as the main silica precursors (Fig. 1). The samples are denoted as M-P-O(-C) with M corresponding to the synthesis method (Imp for impregnation and IS for *in situ*), P to the main

silica precursor used (E for TEOS and M for TMOS), O to the organosilane (EDAS, APTMS or PTMS), and C to the calcination temperature (where relevant).

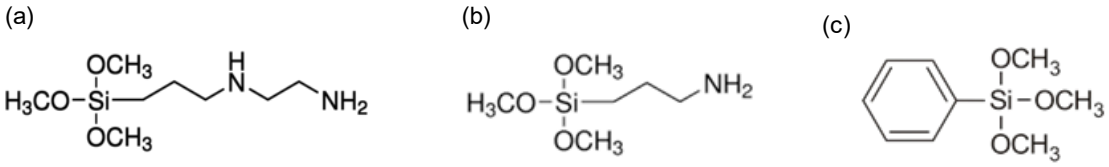

Fig. 1 Chemical structure of (a) EDAS, (b) APTMS, and (c) PTMS

2.2.1. Impregnation method

This procedure was adapted from previous studies [26,49,50]. The samples were synthesized in absolute ethanol, with the main silica precursor (TEOS or TMOS), the organosilane (EDAS, APTMS or PTMS), and 0.9 M (for the Imp-TEOS-PTMS sample) or 0.18 M (for the other samples) aqueous NH_3 solution. Synthesis processing variables were selected in order to adopt a hydrolysis ratio (*i.e.* $[H_2O]/([\text{main silica precursor}]+3/4[\text{organosilane}])$) equal to 5, a dilution ratio (*i.e.* $[C_2H_5OH]/([\text{main silica precursor}] + [\text{organosilane}])$) equal to 10, and a ratio of organosilane to main silica precursor (*i.e.* [organosilane]/[main silica precursor]) equal to 0.2. This provided a molar ratio main silica precursor:organosilane:ethanol:water:NH_3 of 157:31.5:1890:903:2.9. Table 2 presents the different samples obtained using the impregnation method.

The main silica precursor was first mixed with ethanol (68 mL) under stirring at room temperature. The organosilane was then added under constant stirring. Ethanolic NH_3 solution (20.1 mL of 0.18 M or 0.9 M aqueous NH_3 solution in 68 mL of ethanol) was finally added to the mixture under vigorous stirring. The volume of the final solutions was about 200 mL. For the gelation and ageing steps, the sample vessel was closed and heated to 80°C for 72 h. Then, the resulting gels were dried under air at room temperature for 72 h. The gels were further dried under vacuum by placing the open vessel in an oven at 150°C and 50 Pa for 24 h. Samples were finally calcined by heating up

to 450°C at a rate of 2°C/min for 12 h and then at 550°C for 12 h at a rate of 2°C/min. Imp-E-EDAS, Imp-E-APTMS, Imp-E-PTMS, and Imp-M-EDAS samples were obtained after drying and Imp-E-EDAS-550 after calcination at 550°C, as shown in Table 2.

After the synthesis, the samples were ground and the powder fraction between 300 and 700 µm was kept for further treatments and characterization. This fraction was impregnated in a STI solution (1 mg/mL in PBS) for 72 h at 25°C under agitation. The mass of the samples was adjusted to obtain a specific surface loading of 10,000 m^2/L. The impregnation was undertaken in duplicates. The suspensions were then centrifuged at 3000 rpm for 5 min and the supernatants were removed. The particles were finally freeze-dried for 3 days. The resulting samples were stored at -20°C.

Table 2 – Synthesis conditions of the silica gels samples via impregnation method.

Sample	Main silica precursor (g)	Organosilane (g)	Calcination
Imp-E-EDAS-550	46.5	8.3	550°C
Imp-E-EDAS	46.5	8.3	No
Imp-M-EDAS	28.2	8.3	No
Imp-E-APTMS	46.5	6.7	No
Imp-E-PTMS	46.5	6.7	No

Note: in the sample name "Imp-X-Y", X corresponds to the main silica precursor (E for TEOS and M for TMOS) and Y to the organosilane (EDAS, APTMS, or PTMS).

2.2.2. *In situ* method

This procedure was adapted from Reiner *et al*. [23]. The samples were synthesized in PBS, with TMOS, organosilane (EDAS, APTMS or PTMS), and 2.5 mM aqueous HCl solution. TEOS could not be used in this case because this compound is insoluble in water [25]. Synthesis processing variables were fixed using a prehydrolysis ratio (*i.e.* $[H_2O]_{prehydrolysis}$/[TMOS]) equal to 1.25, a total dilution ratio (*i.e.* ($[H_2O]_{prehydrolysis}$+$[H_2O]_{PBS}$)/([TMOS]+[organosilane]) equal to 19.3, and a ratio of organosilane to TMOS (*i.e.* [organosilane]/[TMOS]) equal to 0.2. This provided a molar ratio TMOS:water:HCl of 78:1510:4.40 x 10^{-3} in the case of IS-M sample and a molar ratio

TMOS:organosilane:water:HCl of 78:16:1736:4.40 x 10^{-3} for IS-M-EDAS, IS-M-APTMS, and IS-M-PTMS samples. Table 3 presents the different samples obtained using the *in situ* method.

TMOS (9.7 g) was first prehydrolyzed in aqueous HCl solution (1.47 mL, 2.5 mM) at room temperature for 30 min under stirring. The organosilane and the STI solution (5 mg/mL in PBS) were then added under stirring. For the gelation and ageing steps, the sample vessel was sealed and left at room temperature for 72 h. The gels were finally dried under air at room temperature for 72 h. No calcination was performed in this case to avoid the protein degradation.

The resulting materials were ground into powders and the fraction sized between 300 and 700 µm was stored at -20°C. Protein-free gels (Blank) were prepared by replacing the protein PBS solution by a protein-free PBS solution. The silica gels containing the protein are designated via the indication "-Prot" while the silica gels without the protein are designated via the indication "-Blank".

Table 3 – Synthesis conditions of the silica gels samples via *in situ* method.

Samples	Organosilane (g)	STI solution (mL)
IS-M	None	21.20
IS-M-EDAS	2.90	24.58
IS-M-APTMS	2.34	24.58
IS-M-PTMS	2.58	24.58

Note: in the sample name "IS-X-Y", X corresponds to the main silica precursor (M for TMOS) and Y to the organosilane (EDAS, APTMS, or PTMS).

2.3. Sample characterization

2.3.1. Physicochemical characterization

The physicochemical characterization of the samples was performed on the samples without protein, except for the nitrogen adsorption-desorption measurements, which were also carried out on the IS samples containing the protein.

The presence of specific functional groups was confirmed by Fourier transform infrared (FTIR) spectroscopy in ATR mode using an IRAffinity-1 from Shimadzu. The following instrumental settings were used: absorbance, range from 4000 to 400 cm^{-1}, 30 scans, resolution of 2 cm^{-1}. The spectra were normalized to the peak corresponding to Si-O-Si stretching (around 1050-1060 cm^{-1}). The organic content was determined by thermogravimetric analysis (TGA, TGA 7 from Perkin-Elmer) under air atmosphere with a heating rate of 20°C/min between 50°C and 90°C and 10°C/min between 90°C and 900°C. The weight loss was measured between 150°C and 900°C.

The textural properties were characterized by nitrogen adsorption-desorption isotherms in an ASAP 2420 multi-sampler adsorption-desorption volumetric device from Micromeritics. From these isotherms, the microporous volume (V_{DR}) and the equivalent microporous surface (S_{DR}) were calculated using Dubinin-Radushkevich theory [51]. The specific surface area was evaluated using Brunauer, Emmett, and Teller theory (S_{BET}) [51,52]. The mesoporous volume and surface were determined by Barrett, Joyner, and Halenda theory (V_{BJH} and S_{BJH}) [52].

The point of zero charge (PZC) was determined by the method of equilibrium *pH* at high loading [53]. The mass of the samples was first adjusted to obtain a surface loading equal to 10,000 m^2/L in 20 mL (in line with previous studies [53,54]). The porous solids were then soaked for 3 h under stirring in 20 mL of water solutions of various starting *pH* ranging from 1 to 13, adjusted using HCl or NaOH solutions. After equilibration, the equilibrium *pH* was measured using an InLab Expert Pro-ISM electrode from Mettler Toledo. The PZC of the solid corresponds to a plateau in a plot of the final *pH vs.* the initial *pH* [53].

2.3.2. Biochemical characterization

The biochemical characterization of the samples was performed on the samples containing protein. For the impregnation method, protein loading within silica was evaluated by measuring the STI concentration remaining in the supernatant after 72 h of incubation via size exclusion

chromatography using STI as standard. Chromatographic conditions were as follow: PL aquagel-OH 30 8 µm column (8 µm, 300 x 7.5 mm), using 1.45 mM Na_2HPO_4 / 0.55 mM NaH_2PO_4 / 150 mM NaCl buffer as mobile phase at a flow rate of 1 mL/min (pump: System gold 126 from Beckman Coulter) at 30°C (oven: Mystral from Spark Holland) with a UV detection performed at 210 nm (UV detector: System gold 166 from Beckman Coulter). For the *in situ* method, it was assumed that the entire quantity of the protein was encapsulated inside or at the surface of the silica. Hence, the amount of encapsulated protein was based on the amount of sample produced and the amount of STI added during the synthesis.

The kinetics of STI release was determined by immersing the samples in 5 mL of PBS solution in closed vials. The mass of the samples was adjusted to obtain a specific surface loading of 15,000 m^2/L. This analysis was performed in duplicates. Gels were incubated at 37°C under stirring in a water bath. At scheduled times (*i.e.* 30 min, 4 h, 1 day, 1 week, 2 weeks, 4 weeks, 12 weeks), samples were centrifuged at 1000 rpm for 5 min. The supernatants were removed, stored at -20°C until analysis, and replaced by fresh PBS. The STI concentration was assessed via the size exclusion chromatography technique as described above.

3. RESULTS AND DISCUSSION

3.1. Gel synthesis

From a macroscopic point of view, the two synthesis processes produce monoliths which were subsequently ground into 300-700 µm particles. Several comments can be made regarding the synthesis processes. Regarding the synthesis processes, a higher concentration of NH_3 was used in the Imp-E-PTMS sample synthesis compared to the samples synthesized with EDAS or APTMS to promote gelation. This is probably due to the absence of amine groups on PTMS, which further catalyze the reaction [55]. The nature of the organosilane also influences the speed of gelation. Regarding the impregnation process, the gelation occurs in 15 min for TEOS + APTMS, in 32 min

for TEOS + EDAS, in 180 min for TEOS + PTMS, and in 55 min for TMOS + EDAS. In contrast, the gelation for the *in situ* synthesis occurred more rapidly. Indeed, the gelation occurred in less than 5 s in the case of EDAS and APTMS, in 70 s in the case of PTMS, and in 90 s without the addition of organosilane. This is directly linked to the use of TMOS, which is more reactive than TEOS, and to the presence of the prehydrolysis step [25].

3.2. Composition of samples

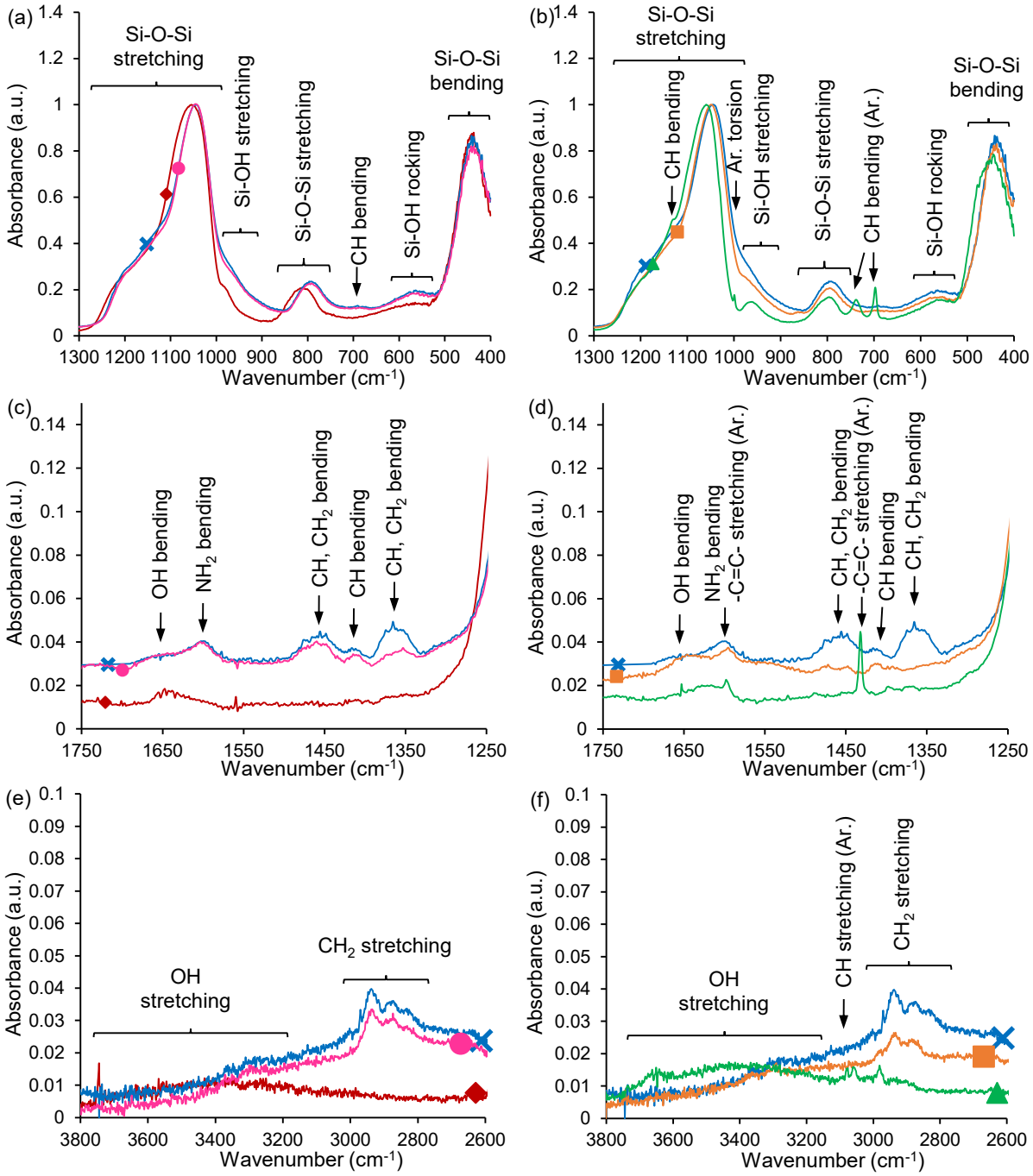

Fig. 2 FTIR spectra of the silica gels produced via the impregnation method: ◆ Imp-E-EDAS-550, ✕ Imp-E-EDAS, ● Imp-M-EDAS, ■ Imp-E-APTMS, ▲ Imp-E-PTMS. (a-b) Zone 400-1300 cm^{-1}, (c-d) zone 1250-1750 cm^{-1}, (e-f) zone 2600-3800 cm^{-1}. Ar = Aromatic ring

The FTIR absorbance spectra of the silica gels are displayed in Fig. 2Fig. 3. All FTIR spectra exhibit characteristic peaks of silica (Fig. 2 (a-b)Fig. 3 (a)). The peaks corresponding to the bending mode of Si-O-Si groups are observed at 440-444 cm^{-1} [56–58]. The stretching modes of Si-O-Si groups are detected at 785 and 810 cm^{-1} (*i.e.* symmetric stretching), between 1030 and 1060 cm^{-1} (*i.e.* transverse optical mode of antisymmetric stretching), and in the 1110-1300 cm^{-1} range (*i.e.* longitudinal optical mode of antisymmetric stretching) [57–60]. The stretching modes of Si-O-Si groups are detected at higher wavenumber for the silica gels without functional group compared to those with functional groups. For example, the respective peaks for the Imp-E-EDAS-550 sample are 810, 1054, and 1120-1300 cm^{-1} while these values shifts toward lower wavenumbers for the Imp-E-EDAS sample (*i.e.* 792, 1044, and 1100-1250 cm^{-1}). This shift is related to the deformation of the network in order to incorporate the organic groups within the silica matrix (*i.e.* greater Si-O-Si angles and Si-O bond lengths) [59]. Characteristics peaks of silanol groups are found at 544-568 cm^{-1} (*i.e.* rocking mode of Si-OH groups) and around 870-990 cm^{-1} (*i.e.* antisymmetric stretching mode of Si-OH groups) [56,58–60]. These bands are less marked in the case of the Imp-E-EDAS-550 sample compared to the other impregnated samples. This can be explained by the condensation of adjacent silanols into siloxane bonds during the calcination [61,62].

The presence of $–(CH_2)_3$-NH-$(CH_2)_2$-NH_2 groups is revealed in the Imp-E-EDAS (Fig. 2 (c-f)Fig. 3 (b-c)), Imp-M-EDAS, and IS-M-EDAS samples by the presence of peaks corresponding to C-H bond (*i.e.* bending at 687-698 cm^{-1}, 1355-1365 cm^{-1}, 1410-1415 cm^{-1}, and 1450-1475 cm^{-1}), $–CH_2$ groups (*i.e.* bending at 1355-1365 cm^{-1} and 1450-1475 cm^{-1}, stretching at 2800-3000 cm^{-1}), and $–NH_2$ groups (*i.e.* bending at 1600 cm^{-1}) [59,63,64]. After calcination at 550°C, these organic groups are replaced by –OH groups [56–59,63]. The characteristic peaks of $–(CH_2)_3NH_2$ are observed for the Imp-E-APTMS and IS-M-APTMS samples (Fig. 2 (c-f)Fig. 3 (b-c)) via the C-H bond (*i.e.* bending at 687 cm^{-1}, 1365 cm^{-1}, and 1410 cm^{-1}), the $–CH_2$ groups (*i.e.* bending at 1470 cm^{-1},

stretching at 2800-3000 cm^{-1}), and $–NH_2$ groups (*i.e.* bending at 1595 cm^{-1}). Finally, the $–C_6H_5$ are detected in the Imp-E-PTMS and IS-M-PTMS samples (Fig. 2 (c-f)Fig. 3 (b-c)) through the C-H bond (*i.e.* bending at 697 cm^{-1}, 740 cm^{-1}, and 1126 cm^{-1} and stretching at 3050 cm^{-1}), the aromatic ring (*i.e.* torsion at 697 cm^{-1} and 999 cm^{-1}), and –C=C– groups (*i.e.* stretching at 1432 and 1600 cm^{-1}) [59,63–67]. –OH groups are also found (*i.e.* bending around 1630-1650 cm^{-1} and stretching around 2700-3700 cm^{-1}) [56–59,68]. Regarding the IS-M sample, only characteristic peaks of silica and –OH groups are observed. These –OH groups are probably due to presence of water in the silica pore.

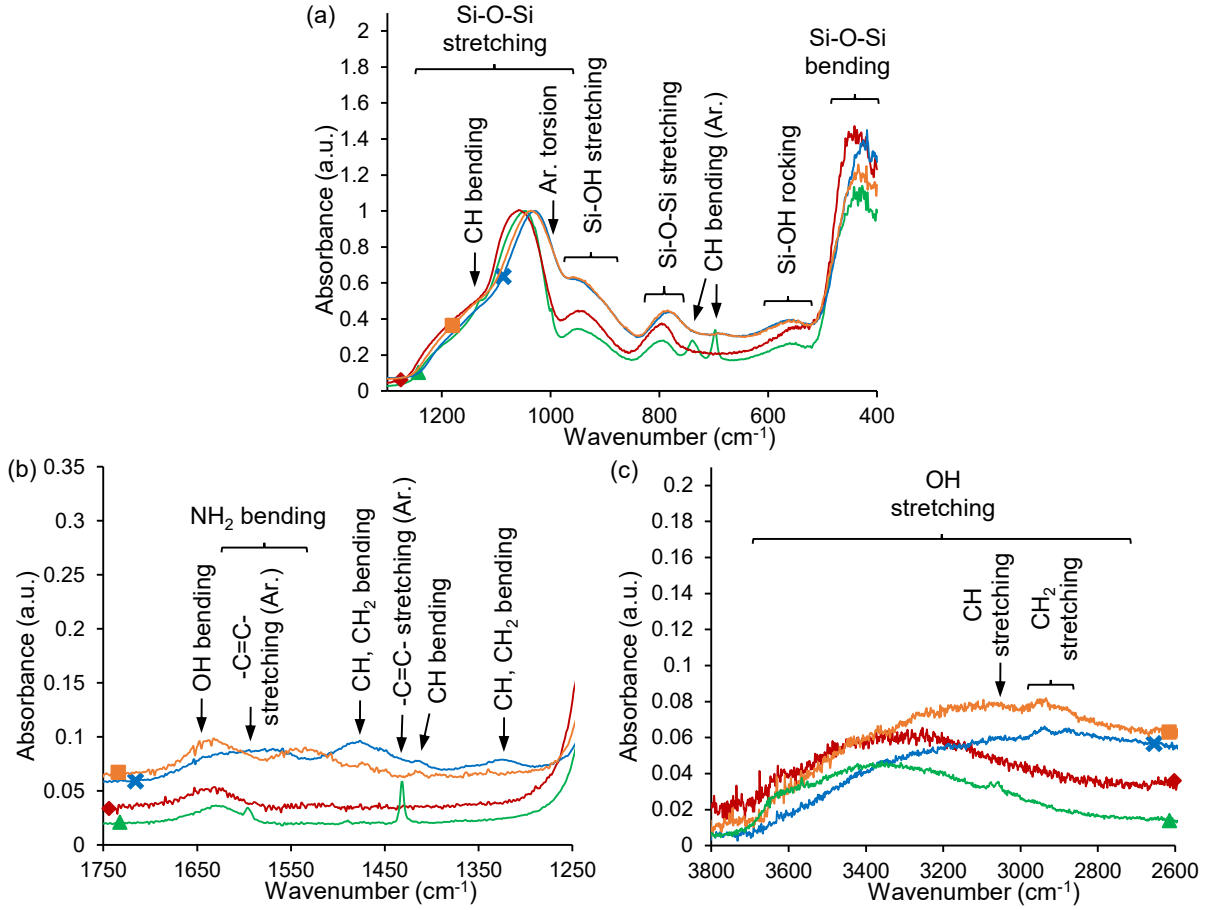

Fig. 3 FTIR spectra of the silica gels produced via the *in situ* method: ◆ IS-M, ✕ IS-M-EDAS, ■ IS-M-APTMS, ▲ IS-M-PTMS. (a) Zone 400-1300 cm^{-1}, (b) zone 1250-1750 cm^{-1}, (c) zone 2600-3800 cm^{-1}. Ar = Aromatic ring

The percentage of organic content in the functionalized silica samples was determined by TGA (Table 4). For both synthesis methods (impregnation and *in situ*), modified samples exhibit a large weight loss due to the presence of organic groups at the surface of the pores. The organic content depends on the nature of the organosilane and, more specifically, on the molar mass of the pendent group. For all modified samples, the experimental weight loss related to organic content is between 4.65 and 6.02 mmol/g, which is close to the theoretical value (Table 4). The slight increase of the experimental weight loss compared to the theoretical value can be explained by the condensation of adjacent silanols [61,62]. Regarding the effect of the nature of the main silica precursor, the results show similar results for the Imp-E-EDAS and Imp-M-EDAS samples.

Table 4 – TGA analysis of the silica gels.

Sample	Experimental weight loss (wt%)	Theoretical weight loss (wt%)	Concentration (mmol/g)
Imp-E-EDAS-550	5	/	5.70
Imp-E-EDAS	24	22.7	4.65
Imp-M-EDAS	24	22.7	4.67
Imp-E-APTMS	17	14.4	5.97
Imp-E-PTMS	22	18.2	5.52
IS-M	8	/	9.00
IS-M-EDAS	25	22.7	4.84
IS-M-APTMS	18	14.4	6.02
IS-M-PTMS	21	18.2	5.41

Note: / = not relevant

Regarding the impregnation method, the results show that the thermal post-treatment also influences the organic content, as observed in the FTIR spectra. The Imp-E-EDAS-550 sample exhibits a much lower organic content compared to the corresponding dried sample (*i.e.* Imp-E-EDAS sample) because of the combustion of ethylene diamine groups during the calcination step. Nevertheless, the measured weight loss may be attributed to the condensation of adjacent silanols at high temperatures, with the formation of siloxane bonds and the release of water molecules

[61,62]. The value observed corresponds to a concentration of 6.3 –OH groups/nm², which is in agreement with those obtained by Zhuravlev *et al*. [69]. Regarding the *in situ* technique, the unexpected weight loss observed for the IS-M sample can be explained by the condensation of silanols. Nevertheless, the value observed corresponds to a concentration of 11.9 –OH groups/nm², which is significantly higher than those obtained by Zhuravlev *et al*. This can be attributed to an incomplete condensation as well as the presence of residual water (drying at room temperature) or salts due to the use of PBS.

3.3. Textural properties

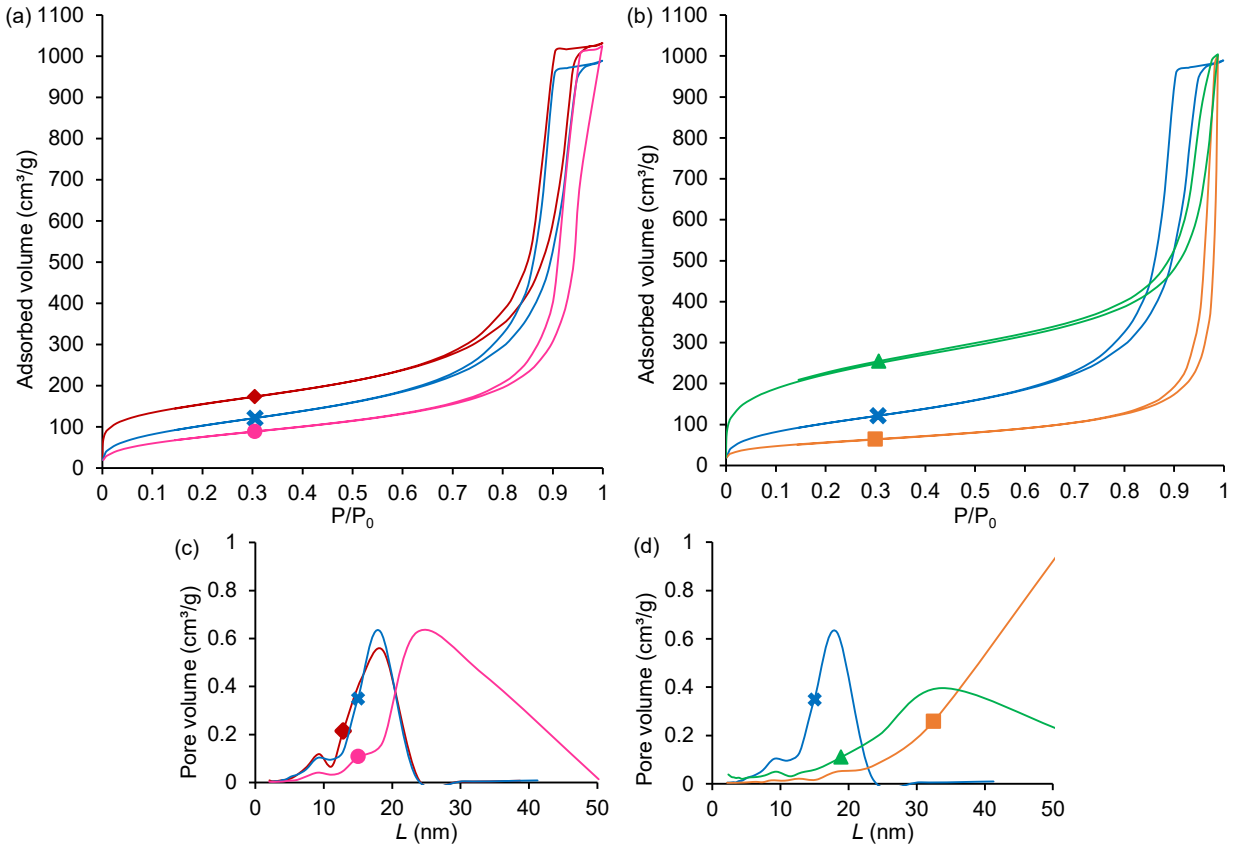

Fig. 4 Nitrogen adsorption-desorption isotherms (a-b) and pore size distributions (c-d) of the silica gels produced via the impregnation method: ◆ Imp-E-EDAS-550, ✖ Imp-E-EDAS, ● Imp-M-EDAS, ■ Imp-E-APTMS, ▲ Imp-E-PTMS

The nitrogen adsorption-desorption isotherms are depicted in **Erreur ! Source du renvoi introuvable.**Fig. 5. Textural properties of all the samples are given in Table 5. It can be observed that the synthesis method, the nature of the main silica precursor, the nature of the organosilane, and the calcination treatment greatly affect the textural properties. Regarding the impregnation method, two types of isotherms are observed. On the one hand, a mixture of Types I and IV isotherms according to the BDDT classification (**Erreur ! Source du renvoi introuvable.** (a-b)) is present for the Imp-E-EDAS-550, Imp-E-EDAS, and Imp-M-EDAS samples, indicating the presence of micro- and mesopores [70]. Type I isotherms are characterized by a sharp increase of the adsorbed volume at low pressure due to the micropore filling (microporous solid) while Type IV isotherms are characterized by the presence of a hysteresis resulting from capillary condensation (mesoporous solid). More specifically, the shape of the hysteresis (*i.e.* Type H2) indicates the presence of large mesopores with narrow mouths (*i.e.* bottle-like pores). The influence of the main silica precursor on the textural properties is observed via a shift of the hysteresis towards higher pressure, indicating an increase in pore size. This is confirmed by the BJH distribution, *i.e.* increase in pore size from 18 nm for the Imp-E-EDAS sample to 23 nm for the Imp-M-EDAS sample and widening of the pore size distribution. Similarly, the specific surface value, S_{BET}, of the Imp-M-EDAS sample (280 m²/g) is lower than that of the Imp-E-EDAS sample (385 m²/g). This can be explained by the mechanism of silica formation and the reaction speed between TEOS/EDAS and TMOS/EDAS. In the case of the Imp-E-EDAS sample, EDAS (which contains methoxy groups) reacts faster than TEOS (which contains ethoxy groups). Consequently, EDAS acts as nucleating agent and forms primary particles on which TEOS condenses in the later stage to form silica particles. This two-step mechanism leads to the formation of silica particles with an EDAS core surrounded by a shell mainly composed of hydrolyzed TEOS [50]. In the case of the Imp-M-EDAS sample, the difference in reactivity between EDAS and TMOS, which both contains methoxy

groups, is much smaller. Therefore, it can be considered that they react at the same time, *i.e*. one-step mechanism in this case. The presence of EDAS, which bears two amine groups, increases the basicity at the molecular level. The higher *pH* increases the hydrolysis speed of reaction with the production of a high number of nuclei. These nuclei are densely packed, explaining the lower specific surface area value, S_{BET} of the Imp-M-EDAS sample.

The effect of calcination can be analyzed by comparing the Imp-E-EDAS and Imp-E-EDAS-550 samples. The lower specific surface area value observed for the Imp-E-EDAS sample (*i.e*. 385 m^2/g) in comparison to the Imp-E-EDAS-550 sample (540 m^2/g) is explained by the presence of the ethylene diamine groups inside the pores. These groups are degraded after calcination at 550°C, which increases the specific surface area of the Imp-E-EDAS-550 sample. These values are in concordance with previous studies [26,40,50,71].

The nature of the organosilane also has a great impact on the textural properties. Indeed, whereas a mixture of Types I and IV isotherms according to the BDDT classification are observed in the case of the Imp-E-EDAS sample, a mixture of Types I, II, and IV isotherms are detected for the Imp-E-APTMS and Imp-E-PTMS samples (**Erreur ! Source du renvoi introuvable.** (c-d)) [70]. Type I and IV isotherms, respectively indicative of micro- and mesopores, have already been described earlier in this section. Type II isotherms show a fast increase at high pressure arising from unrestricted monolayer-multilayer adsorption up to high relative pressure, characteristic of a macroporous solid. The Imp-E-APTMS and Imp-E-PTMS samples are therefore composed of micro-, meso-, and macropores. The shape of the hysteresis (*i.e*. Type H3) can be explained by the presence of plate-like particles but more certainly by macropores not completely filled with pore condensate. This is confirmed by the BJH distribution with the existence of a large peak at 33 nm continuing above 50 nm for the Imp-E-PTMS sample (*i.e*. presence of large mesopores and macropores) and a peak above 50 nm for the Imp-E-APTMS sample (*i.e* presence of large

mesopores and of a large proportion of macropores). Interestingly, the S_{BET} values (Table 5) follow the size of the organic moiety of the organosilane, *i.e.* Imp-E-PTMS > Imp-E-EDAS > Imp-E-APTMS. This phenomenon is attributed to the steric hindrance of the functional groups, which affects the space between nuclei [72]. A larger size of the functional group leads to a larger steric hindrance, which in turn results in larger spaces between nuclei and, hence, a higher S_{BET} value.

For the *in situ* method, the sample with and without loaded proteins have been analyzed to study the potential templating effect of the protein. In both cases, a mixture of Types I and IV isotherms is present, which indicates the presence of micro- and mesopores (Fig. 5) [70]. In contrast to the impregnation method, the smaller size of the hysteresis and the presence of a plateau prior to saturation suggest a much lower proportion of mesopores compared to micropores [51,52]. This is confirmed by the BJH distribution with a large proportion of micropores (*i.e.* pore size below 2 nm) and mesopores with a size smaller than 4 nm (*i.e.* distribution around 3.5 nm for the IS-M and IS-M-PTMS samples and around 3.9 nm for the IS-M-EDAS and IS-M-APTMS samples). In the case of the samples without proteins, the pores with a size larger than 4 nm (*i.e.* the protein size) represent between 5 and 20 % of the total pore volume. However, in the case of the samples with the proteins, these pores only represent 5-7 % of the total pore volume. This small proportion of pores larger than the proteins can greatly affect the diffusion of the proteins by notably leading to the total entrapment of the proteins inside the matrix. These results are in contrast to those obtained by Reiner *et al*.. These authors studied the encapsulation and release of STI from unmodified silica synthesized via an *in situ* method similar to the one used in this present study [23]. They showed the presence of pores smaller than 5 nm (no BET isotherm). However, due to the small proportion of mesopores, it is likely that the authors neglected them.

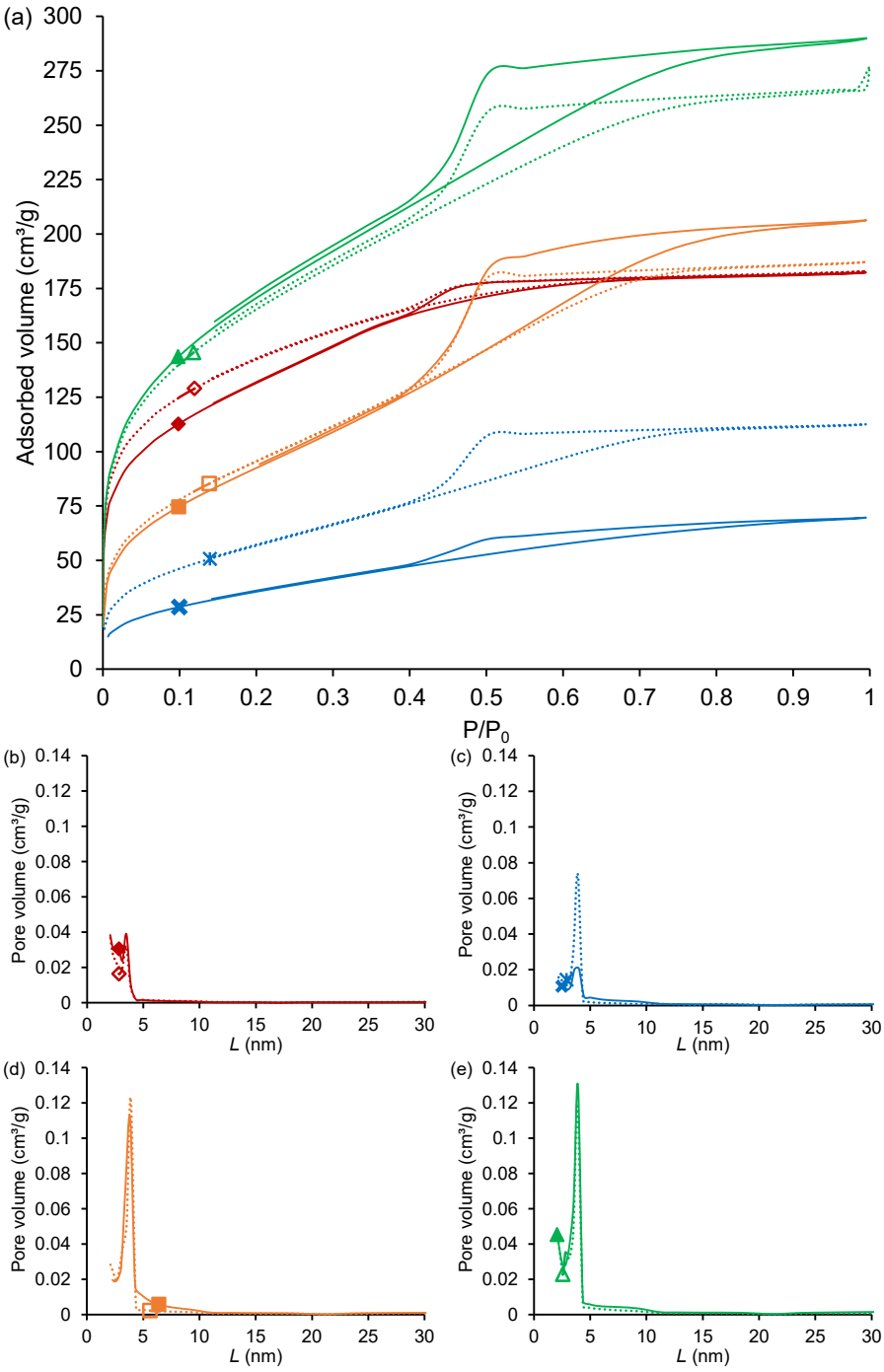

Fig. 5 Nitrogen adsorption-desorption isotherms (a) and pore size distributions (b-e) of the silica gels produced via the *in situ* method. The full symbols and continuous lines correspond to the samples without the proteins and the empty symbols and dashed lines correspond to the samples with the proteins; ◆ IS-M, ✕ IS-M-EDAS, ■ IS-M-APTMS, ▲ IS-M-PTMS

A similar behavior is observed in the samples obtained by the *in situ* method where the nature of the organosilane also has a significant impact on the textural properties. The IS-M sample can be taken as the reference point. In this synthesis, TMOS and organosilanes, which both have methoxy groups, reacts at the same time [50]. Compared to pure TMOS (*i.e.* IS-M sample), the presence of amine groups in the organosilanes increases the hydrolysis rate of reaction by acting as catalysts, leading to the production of densely packed nuclei (as shown for the Imp-M-EDAS sample). This factor explains the lower specific surface area value, S_{BET}, observed for the IS-M-EDAS (130 m²/g) and IS-M-APTMS (350 m²/g) samples compared to that of IS-M (455 m²/g). The even lower S_{BET} value of the IS-M-EDAS sample compared to that of the IS-M-APTMS sample is due to the higher number of amine groups present on the organosilane, *i.e.* two amine groups for EDAS and one amine group for APTMS. For the IS-M-PTMS sample, as mentioned for the Imp-E-PTMS sample, the higher S_{BET} (605 m²/g) observed compared to the others is probably due to a steric effect of the phenyl group during the nucleation step.

Regarding the BJH method for the IS samples, it is noteworthy to indicate that the S_{BJH} and V_{BJH} values summarized in Table 5 are overestimated and not representative of the samples. Indeed, the BJH method considers a perfectly mesoporous solid while the IS samples exhibits a large proportion of micropores. However, they can be analyzed from a qualitative point of view, confirming a larger amount of mesopores for the IS-M-APTMS and IS-M-PTMS samples, compared to the IS-M and IS-M-EDAS ones.

Table 5 – Textural properties of the silica gels.

Sample	S_{BET} (m^2/g) ± 5	V_P (cm^3/g) ± 0.1	V_{DR} (cm^3/g) ± 0.01	V_{BJH} (cm^3/g) ± 0.01	S_{BJH} (cm^2/g) ± 5
Imp-E-EDAS-550	540	1.6	0.25	1.60	535
Imp-E-EDAS	385	1.5	0.21	1.51	490
Imp-M-EDAS	280	1.6	0.16	1.57	345
Imp-E-APTMS	205	1.5	0.11	1.51	215
Imp-E-PTMS	780	1.5	0.35	1.47	620
IS-M-Blank	455	0.3	0.23	0.22	310
IS-M-Prot	500	0.3	0.23	0.18	255
IS-M-EDAS-Blank	130	0.1	0.08	0.12	140
IS-M-EDAS-Prot	210	0.2	0.12	0.19	235
IS-M-APTMS-Blank	350	0.3	0.18	0.32	370
IS-M-APTMS-Prot	355	0.3	0.18	0.32	395
IS-M-PTMS-Blank	605	0.4	0.28	0.41	505
IS-M-PTMS-Prot	585	0.4	0.27	0.36	460

Note: S_{BET}: specific surface area determined by the BET method; V_P: specific liquid volume adsorbed at the saturation pressure of nitrogen; V_{DR}: specific micropore volume determined by the Dubinin–Raduskevitch theory; V_{BJH}: specific mesoporous volume determined by the Barrett, Joyner, and Halenda theory; S_{BJH}: specific mesoporous surface determined by the Barrett, Joyner and Halenda theory.

Besides the nature of the organosilane, the synthesis method and in particular the *pH* of the synthesis greatly influence the textural properties. To assess this influence, the Imp-M-EDAS and IS-M-EDAS samples are compared because they are composed of the same main silica precursor and organosilane. As presented previously, the Imp-M-EDAS sample (synthesized in basic conditions) exhibits a small proportion of micropores and large mesopores while the IS-M-EDAS sample (synthesized in acidic conditions) present a large proportion of micropores and small mesopores. On the one hand, condensation using a basic catalyst (*i.e.* impregnation method) gives small nanoparticles, which aggregate to form a gel. This tridimensional network exhibits pores between these particles, which explains the presence of mesopores in the Imp-M-EDAS [25]. On the other hand, an acid catalysis (*i.e. in situ* method) gives linear and randomly branched chains which pack together, leading to smaller pores.

3.4. Determination of the Point of Zero Charge (PZC)

The evolutions of the final *pH* as a function of the initial *pH* (Fig. 6) clearly show a plateau for all samples, which corresponds to the Point of Zero Charge (PZC) value (Table 6). The identification of the PZC value allows the surface charge of the samples to be determined, which influences the "silica-protein" interactions and subsequently the protein release kinetics and its activity. When *pH* < PZC, the surface charge of the sample is positive, characteristic of the presence of $–OH_2^+$ and/or $–NH_3^+$ surface groups. In contrast, when *pH* > PZC, the surface charge of the sample is negative, characteristic of the presence of $–O^-$ and/or $–NH^-$ groups [53,54]. Following this reasoning, it is clear that the surface of samples containing amine functions (*i.e.* Imp-E-EDAS, Imp-E-APTMS, Imp-M-EDAS, IS-M-EDAS, IS-M-APTMS samples) is positively charged at the *pH* of the release solution (*i.e.* 7.4, Fig. 6), while the Imp-E-EDAS-550, Imp-E-PTMS, IS-M, and IS-M-PTMS samples exhibit a negative charge at their surface. It is nevertheless worthwhile to notice that the PZC value of the Imp-E-APTMS sample is very close to 7.4, indicating that its surface charge is almost neutral.

The difference in PZC between samples is explained by the surface chemistry and their accessibility. Ethylene diamine present at the surface of EDAS modified samples and amine groups present at the surface of APTMS modified samples are responsible for the high PZC value, as observed in Fig. 6 (pK_a for the protonation of the amine groups into the corresponding ammonium form equal to 9.6) [62]. The accessibility of the amine groups is also important. When TMOS is used as the main silica precursor, it simultaneously reacts with the organosilane, leading to a high accessibility of the functional groups and a high PZC value. In contrast, when TEOS is used as main silica precursor, the organosilane reacts before TEOS, leading to particles formed by an organosilane core surrounded by a TEOS shell. The functions are thus not as accessible as in the samples synthesized with TMOS. For the samples synthesized using the impregnation method, a

higher PZC would therefore be expected for the Imp-M-EDAS sample than for the Imp-E-EDAS one. Nevertheless, in the case of large organosilane/TEOS ratios, Alié *et al*. have observed the presence of accessible amine groups due to a partial covering of the amine groups by relatively small quantities of SiO_2 generated by hydrolysis and condensation of TEOS [55]. Following the same reasoning, the difference between the Imp-E-EDAS and Imp-E-APTMS samples can be explained by different covering of the R-$SiO_{1.5}$ from the organosilane by SiO_2 from TEOS, leading to differences in amine accessibility. For the samples synthesized with the *in situ* method, a PZC value comparable to that of Imp-M-EDAS would be expected. Yet, the lower PZC observed can be attributed to a larger amount of silanol groups. These groups are more acidic, leading to a lower PZC value. The PZC values measured for samples with accessible amine groups are in good agreements with those disclosed in the literature (*i.e*. PZC around 9-10) [62].

Regarding the other samples, the presence of silanol groups and siloxane bridges at their surface explains the lower PZC value (*i.e*. between 5.4 and 6.5). Compared to the literature, the value measured for the Imp-E-EDAS-550 and IS-M samples is higher than the ones found for bare silica (*i.e*. PZC = 2-3) [73]. This behavior indicates a larger proportion of siloxane groups (less acidic) than silanol groups (more acidic) in these samples compared to bare silica [62]. For the Imp-E-EDAS-550 sample, this larger proportion can be explained by the complete condensation of adjacent silanols at high temperature [61,62]. For the IS-M sample, the presence of residual salt from the PBS leads to an increase in the PZC, which reaches 6.5. For the Imp-E-PTMS and IS-M-PTMS samples, the influence of the silanol groups and siloxane bridges is tempered by the neutral phenyl groups, leading to slightly higher PZC (*i.e*. 6.8-7) than the one of the Imp-E-EDAS-550 and I-M samples.

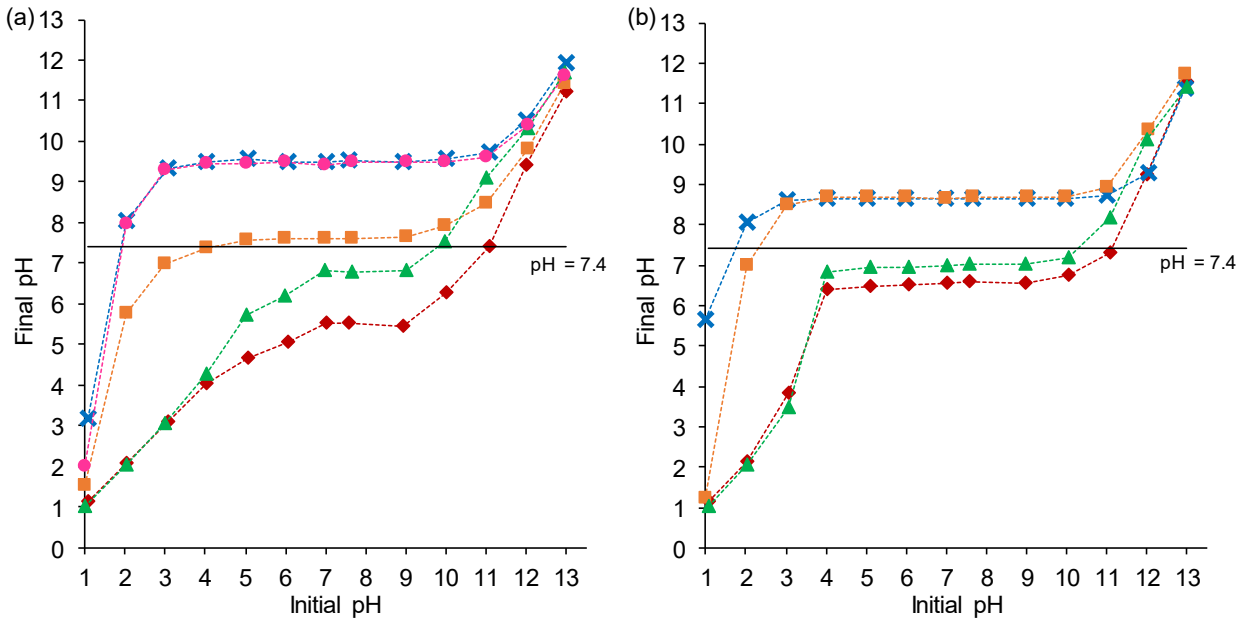

Fig. 6 PZC determination of the silica gels produced via (a) the impregnation method: ◆ Imp-E-EDAS-550, ✕ Imp-E-EDAS, ● Imp-M-EDAS, ■ Imp-E-APTMS, ▲ Imp-E-PTMS; and (b) the *in situ* method: ◆ IS-M, ✕ IS-M-EDAS, ■ IS-M-APTMS, ▲ IS-M-PTMS. The full line represents the pH of the release solution (*i.e.* pH = 7.4)

Table 6 – PZC values of the silica gels.

Sample	Experimental
Imp-E-EDAS-550	5.4
Imp-E-EDAS	9.5
Imp-M-EDAS	9.5
Imp-E-APTMS	7.6
Imp-E-PTMS	6.8
IS-M	6.5
IS-M-EDAS	8.7
IS-M-APTMS	8.7
IS-M-PTMS	7.0

3.5. Protein encapsulation

The amount of encapsulated STI per unit mass of silica or per unit of specific surface area of silica is presented in Fig. 7. It is observed that the amount of encapsulated STI greatly varies among samples. This heterogeneity is specifically observed for the impregnation method with a 8.6-fold difference between the highest (58 mg/g) and lowest (7 mg/g) encapsulated quantity (Fig. 7 (a)).

In particular, PTMS-modified silica (*i.e.* Imp-E-PTMS sample) exhibits the highest amount of encapsulated STI (107 µg/m²) followed by calcined silica (*i.e.* Imp-E-EDAS-550 sample, 43 µg/m²), and the amine-modified samples (*i.e.* Imp-E-EDAS, Imp-E-APTMS, and Imp-M-EDAS samples with 15, 14 and 12 µg/m^2, respectively). Focusing on Fig. 7 (b), this difference in protein loading can be attributed to the specific interactions of the functional groups with the protein, noting that the specific surface area has been kept constant for all samples. Accordingly, these observations indicates that the STI exhibits a high affinity for the phenyl-modified sample (*i.e.* Imp-E-PTMS sample), a medium affinity for the calcined sample (*i.e.* Imp-E-EDAS-550 sample), and a low affinity for the amine-modified samples (*i.e.* Imp-E-EDAS, Imp-M-EDAS, and Imp-E-APTMS samples). These results highlight the hydrophobic character of the protein, which shows a higher affinity for hydrophobic functions such as phenyl groups (*i.e.* Imp-E-PTMS sample) and siloxane bridges (Imp-E-EDAS-550 sample) compared to the hydrophilic ones (*i.e.* Imp-E-EDAS, Imp-M-EDAS, and Imp-E-APTMS samples).

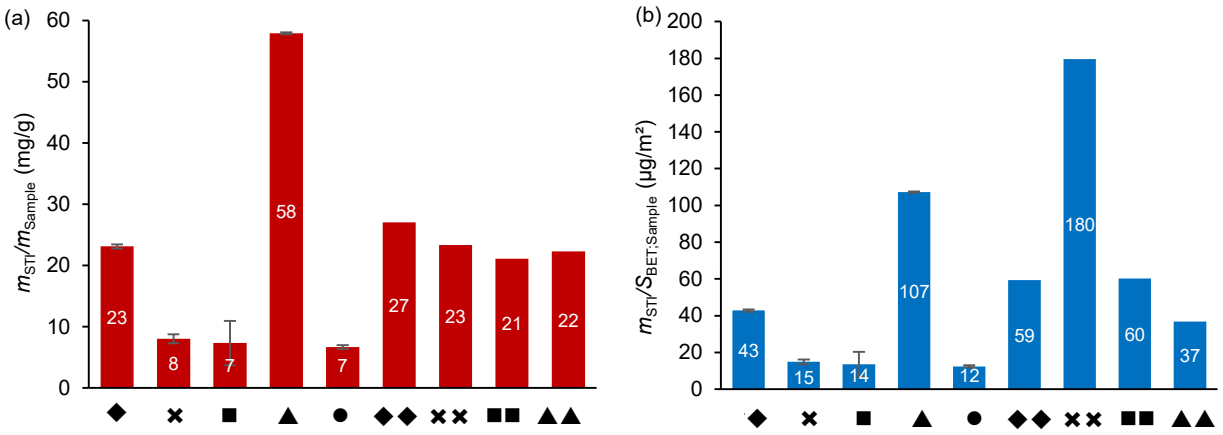

Fig. 7 STI loading expressed as (a) m_{STI}/m_{Sample} and (b) $m_{STI}/S_{BET;Sample}$ in the silica gels synthesized via the impregnation method: ◆ Imp-E-EDAS-550, ✕ Imp-E-EDAS, ■ Imp-E-APTMS, ▲ Imp-E-PTMS, ● Imp-M-EDAS; and the *in situ* method: ◆◆ IS-M, ✕✕ IS-M-EDAS, ■■ IS-M-APTMS, ▲▲ IS-M-PTMS

In the case of the *in situ* method, it is assumed that the entire quantity of STI added during the synthesis has been encapsulated inside or at the surface of the silica matrix. The results (Fig. 7 (a)) show protein loadings (21 to 27 mg/g) close to the value of the Imp-E-EDAS-550 sample (23 mg/g). This quantity is directly fixed by the quantity of STI added during the gel synthesis and can therefore be controlled by regulating the concentration of the STI solution. From Fig. 7 (b), the influence of the specific surface area can be directly seen. The STI loading per unit of specific surface area of silica is in the following order: IS-M-EDAS > IS-M-APTMS > IS-M > IS-M-PTMS. As the quantity of STI is fixed before the synthesis, these results do not depend on specific interactions between the silica and the protein, but instead on the textural properties of the synthesized silica.

It is important to note that these results represent the total amount of protein present inside and at the external surface of the samples.

3.6. Release kinetics profiles

The results presented in section 3.5. show a large heterogeneity in the quantity of protein encapsulated per unit of specific surface area of silica. These will have an impact on the protein release taking into account that, for this study, the specific surface area is kept constant for all samples in order to avoid the influence of the specific surface area. This means that the quantity of protein available at the beginning of the release is different for each sample. In order to rationalize the results, they are presented as the percentage of STI released over time, as shown in Fig. 8 and 9.

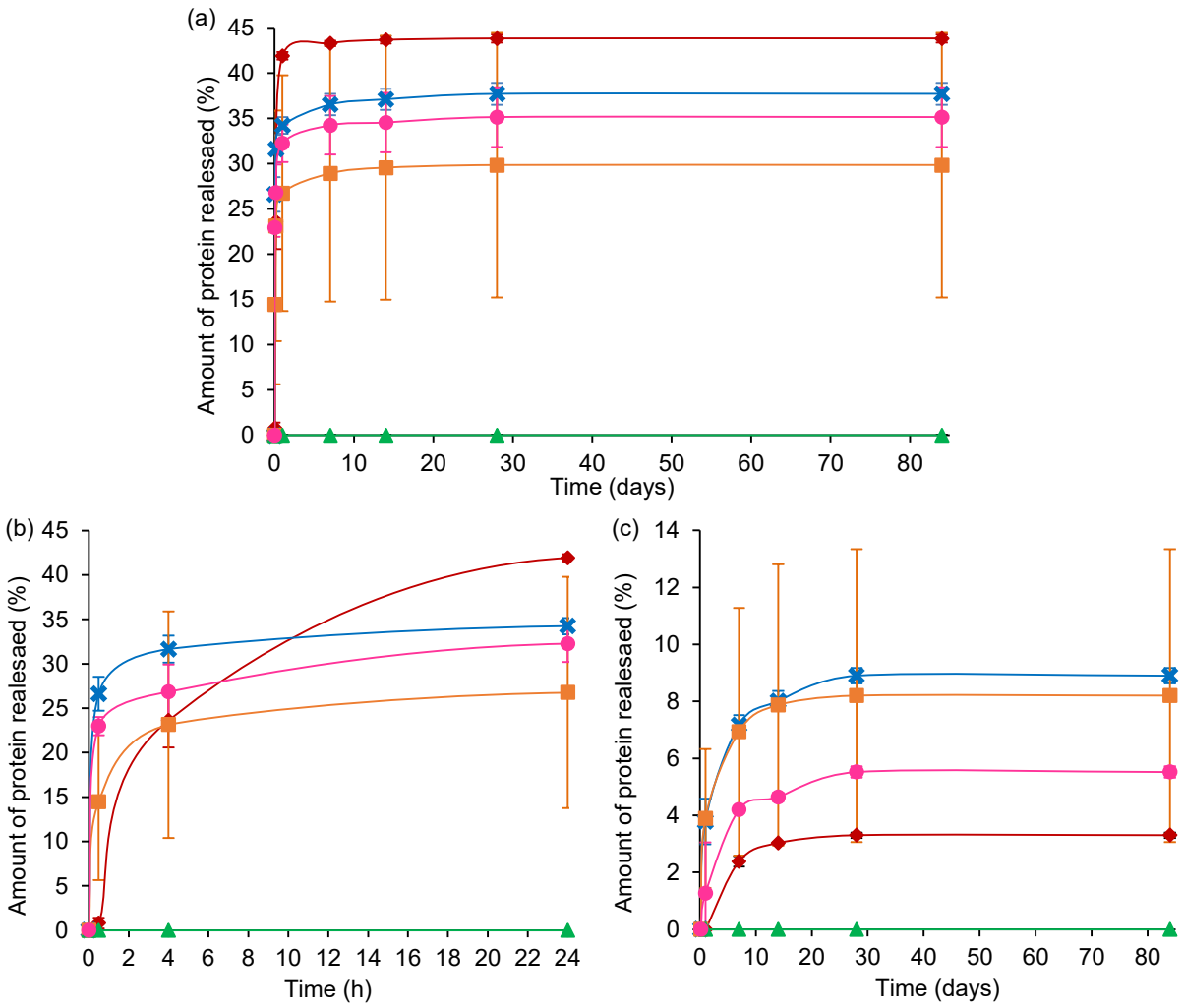

Fig. 8 Release kinetics profile of STI from the silica gels produced via the impregnation method: (a) Release kinetics profile (b) Zoom on the possible burst (0 to 24 h) (c) Profile of the STI released after the first day (STI release up to 24 h is subtracted) ◆ Imp-E-EDAS-550, ✕ Imp-E-EDAS, ● Imp-M-EDAS, ■ Imp-E-APTMS, ▲ Imp-E-PTMS.

Fig. 8 Fig. **9** illustrate the release kinetic profiles. To ensure clarity, these figures are divided in three parts: (a) profiles over 80 days, (b) zoom on the first 24 h of release, and (c) amount of STI released after the first day. This last figure is expressed as the percentage of STI remaining in the silica after day 1, with the STI released up to 24 h being subtracted.

Before discussing the two synthesis methods separately, it is important to mention that PTMS-modified samples (*i.e.* Imp-E-PTMS and IS-M-PTMS samples) do not exhibit a significant release

of STI over the 85 days period. As the proteins would not be accessible, bone regeneration would not benefit from this approach. Yet, taking into account the high amount of STI encapsulated in these samples, these observations suggest a high affinity of the STI for the pendant phenyl groups . Based on these results, new silica synthesis could be developed to modulate the hydrophobicity of the pores in order to allow a protein release. Different strategies could be adopted, such as the nature (*e.g.* phenyl, C18), the concentration, and the position (*i.e.* pendant in the pores vs included inside the walls) of the hydrophobic groups. Moreover, in other applications, this permanent entrapment of proteins could find great interest, particularly in the field of biocatalysis.[74,75]

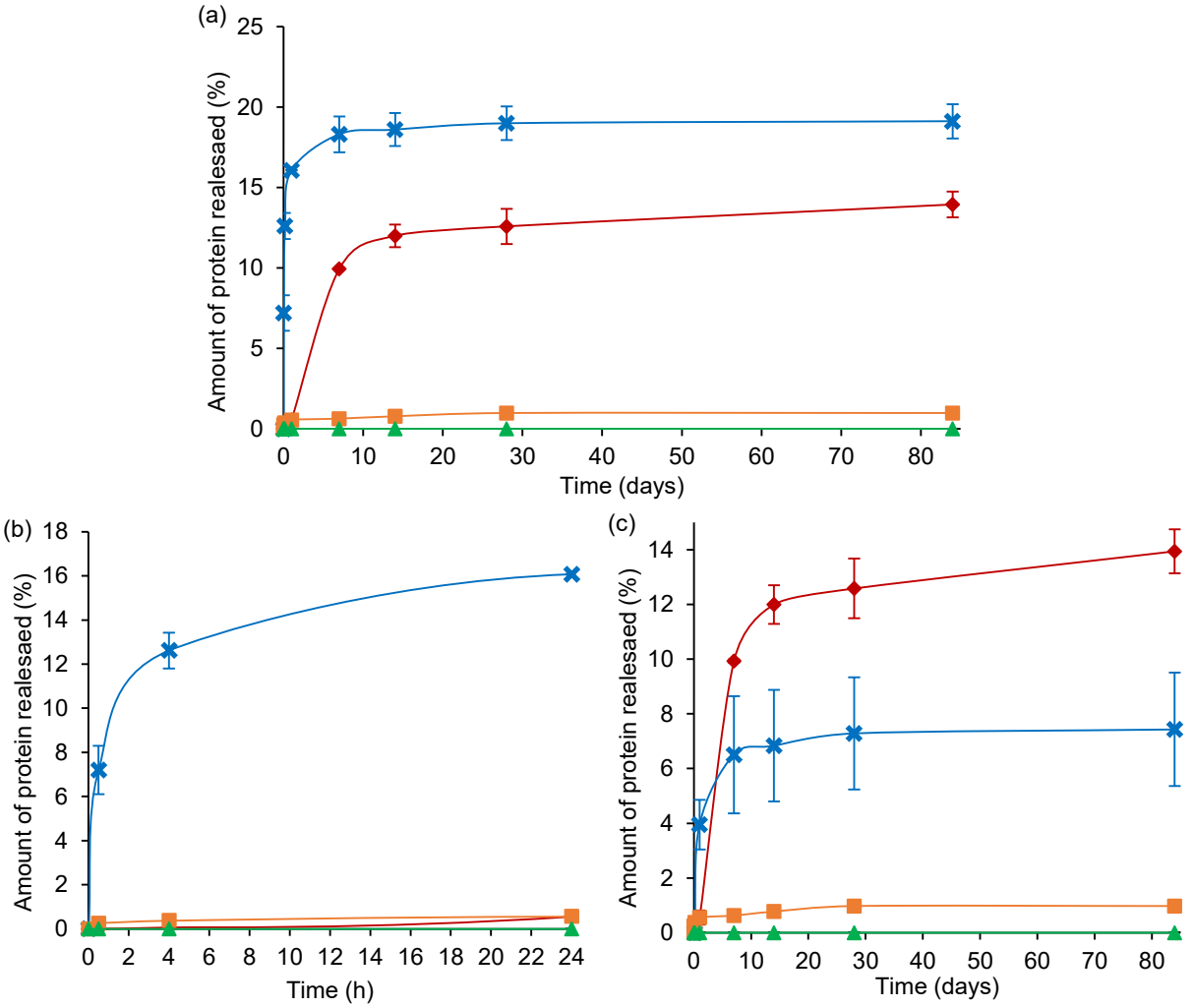

Fig. 9 Release kinetics profile of STI from the silica gels produced via the *in situ* method: (a) Release kinetics profile (b) Zoom on the possible burst (0 to 24 h) (c) Profile of the STI released

after the first day (STI release up to 24 h is subtracted). ◆ IS-M, ✕ IS-M-EDAS, ■ IS-M-APTMS, ▲ IS-M-PTMS

Regarding the samples prepared by impregnation, the release kinetics profiles (Fig. 8) highlight a fast release of STI from the amine-modified samples (*i.e.* Imp-E-EDAS, Imp-M-EDAS, and Imp-E-APMTS samples) within the first 4 h. This burst was also observed for the Imp-E-EDAS-550 samples but over a longer period (*i.e.* within the first 24 h). During this period, between 25 and 40 % of the encapsulated STI are released. It is assumed that this burst is mostly due to the fraction of the protein adsorbed on the external surface of the silica particles, which can easily and rapidly desorb upon immersion. A remark must therefore be expressed regarding the results presented in Fig. 7. These results represent the total amount of protein present inside and at the external surface of the samples. Taking into account the results of this section, it seems that the proteins present at the surface of the silica account for 25 to 40 % of the total amount. This means that the quantity of encapsulated proteins is equal to 5 mg_{STI}/g_{Sample} for the Imp-E-EDAS, Imp-E-APTMS, and Imp-M-EDAS samples and 14 mg_{STI}/g_{Sample} for the Imp-E-EDAS-550 sample. Regarding the Imp-E-PTMS sample, no clear conclusion can be expressed regarding the amount of proteins inside or at the external surface of the sample, as no release could be observed.

Following the rationale that the burst release is probably due to STI adsorbed at the surface, we have focused on the release of STI after the the burst event, which we attribute to protein encapsulated inside the silica pores. We therefore express the rest of the profile as the proportion of the remaining STI after 4 or 24 h that is released in the medium (Fig. 8 (c)). Beyond this period, a sustained release of STI is observed up to day 30. The release profiles then achieve a plateau (*i.e.* release < 0.1% between day 30 and day 85, Fig. 8 (c)), corresponding to 3, 9, 11, and 8 % of the amount of STI remaining after the burst for the Imp-E-EDAS-550, Imp-E-EDAS, Imp-M-EDAS, and Imp-E-APTMS samples, respectively. This STI retention is linked to the interactions between

the STI and functional groups present at the surface of the pores, preventing the total release of the protein. When comparing the samples, a first remark should be made regarding the Imp-E-APTMS sample, which exhibit a high variability between replicates, which is attributed to heterogeneity of this sample. The explanation given above remains valid but this sample is not compared to the others.

The effect of the main silica precursor is analyzed by comparing the samples modified with EDAS (Imp-E-EDAS and Imp-M-EDAS), while the influence of the calcination is determined by comparing the Imp-E-EDAS and Imp-E-EDAS-550 samples. The Imp-E-EDAS sample exhibits slightly faster and higher STI release than the Imp-M-EDAS one. This can be due to their differences in pore size. Indeed, the Imp-E-EDAS sample exhibits smaller pores, which may slow down the protein diffusion compared to the larger pores of the Imp-M-EDAS sample. In contrast, the Imp-E-EDAS and Imp-E-EDAS-550 samples present similar pore size and porous volume. The difference of release profile between these samples can thus be explained by the difference in surface chemistry, more specifically by a higher affinity of STI for hydroxyl groups of the Imp-E-EDAS-550 sample compared to ethylene diamine surface groups of the Imp-E-EDAS sample. The same behavior was already observed by Tang *et al*. for the release of BMP-2 encapsulated in unmodified silica (with only surface hydroxyl species) via an impregnation method [43]. Indeed, these authors showed the presence of a large burst (*i.e*. 20-65 %) followed by a sustained delivery over 28 days.

These findings run counter to those expected from the PZC results. According to the PZC results, the Imp-E-EDAS-550 and Imp-E-PTMS samples bear negative charges at pH = 7.4, while Imp-E-EDAS sample is positively charged at the same pH. As STI is negatively charged at this *pH* (PZC = 4.5), a higher affinity of STI for the positively charged substrate, such as the Imp-E-EDAS sample, would therefore be expected [36]. In practice, both negatively charged samples (*i.e*. Imp-

E-EDAS-550 and Imp-E-PTMS samples) exhibit a higher protein retention than the positively charged one (*i.e.* Imp-E-EDAS sample). The protein retention increases with the hydrophobic character of the samples, with the lowest protein retention being observed for the Imp-E-EDAS sample (bearing hydrophilic ethylene diamine groups), and the highest protein retention for the Imp-E-PTMS (bearing hydrophobic phenyl groups). As observed for protein loading, these results suggest that the hydrophobicity of the matrix should play a larger role on STI encapsulation and release than the surface charges. This predominance in surface hydrophobicity over surface charge has already been reported in the literature [76,77]. These hydrophobic interactions are affected by the surface properties, but also by the protein composition (*i.e.* amino acid nature and sequence), organization and/or its resistance to conformational changes.

In contrast, the IS-M sample exhibits a smaller amount of STI released over the first 24 h, followed by a continuous and large release from day 1 to day 14, and a slow STI release until day 85 (release of 1.3 % between day 30 and day 85, Fig. 9). The slower initial release behavior can be attributed to the fact that all the proteins are encapsulated inside the silica matrix. The subsequent release can be explained by the slow diffusion of the proteins into the small pores of the matrix and a probable liberation of the pores due to the dissolution of salts incorporated in the matrix through the PBS. This behavior was already observed in a previous studies [23,40].

A faster STI release can be observed for the IS-M-EDAS sample (16 % in 24 h). This sample exhibits a lower specific surface area than the other samples, resulting in a higher amount of STI per unit of specific surface area. Therefore, a larger proportion of STI interacts only weakly with the matrix. These proteins can be easily released, causing the burst observed. After this burst, the proteins interacting more strongly with the matrix diffuses out of the pores, as observed for the IS-M sample. After day 30, a plateau establishes at 7 %, *i.e.* release < 0.1 % between day 30 and day 85 (Fig. 9 (a) and (c)). This plateau can be explained by a physical entrapment of STI inside closed

pores, whereas the IS-M sample seems not reached this plateau. Similarly, considering the lower specific surface area and higher STI loaded per unit of specific surface area of the IS-M-APTMS in comparison IS-M-EDAS sample, the higher protein retention in IS-M-APTMS sample may also be related to a larger proportion of STI interacting with the silica matrix.

It is important to notice that these results were obtained in *in vitro* conditions. Nevertheless, previous studies highlighted a fast *in vivo* degradation of silica nanoparticles in zebrafishes, which can also have a strong influence on the protein release [78,79].

4. CONCLUSIONS

In conclusion, silica gels were synthesized via two methods (*i.e.* an impregnation method and an *in situ* method) for the encapsulation and release of STI. A large control of the surface chemistry and textural properties could be obtained through the use of different organosilanes (*i.e.* containing amine, ethylene diamine, or phenyl groups) and main silica precursors (*i.e.* containing methoxy or ethoxy groups). The influence of the nature of the main silica precursors on the textural properties could be observed and was explained by the difference in silica formation (*i.e.* presence or absence of a nucleation process). The nature of the organosilane also largely influenced the textural properties, notably with a large specific surface area for phenyl-containing silica. In general, a large range of pore sizes were measured for silica gels prepared by impregnation (*i.e.* micro-, meso-, and macropores), while the *in situ* silica samples were mainly composed of micro- and mesopores. The surface charge also depended on the nature of the organosilane, with positively charged amine-modified and ethylene diamine-modified samples and negatively charged phenyl-modified and unmodified samples being obtained.

The porosity and surface chemistry of the samples was shown to strongly affect the immobilization and release kinetics profile of STI. In particular, PTMS-modified samples exhibited a high amount

of encapsulated STI accompanied by a very low release of STI over the 85 days period, indicating a high affinity of the protein for the phenyl groups. Based on these promising results, the hydrophobicity of the pores should be tuned by modulating the nature of the hydrophobic groups, their concentration, and their accessibility. The other functional groups (ethylene diamine and amine) gave rise to a lower STI encapsulation. Regarding the release profiles, a fast release of STI was observed during the first 24 h for the impregnated samples, followed by a sustained release until day 30 day. In contrast, the *in situ* method allowed a better control of the STI release over the first 24 h followed by a sustained release up to 85 days.

5. ACKNOWLEDGMENTS

Funding: This work was supported by the Belgian Fund for Scientific Research (FNRS) under a Fund for Research Training in Industry and Agriculture (FRIA) grant, the "Ministère wallon de la Recherche et de l'Innovation", the Interreg VA Grande Région program, and the Wallonia region.

Stéphanie D. Lambert and Ana P. F. Monteiro thank the F.R.S.-FNRS for their Senior Research Associate position and Postdoctoral Researcher position, respectively. Rémi G. Tilkin and Nicolas Régibeau also thank the F.R.S.-FNRS for their FRIA grant.

The authors would like to thank Camille Tilkin for her corrections.

6. CONFLICT OF INTEREST

The authors declare that there is no conflict of interest concerning this work.

7. REFERENCES

1. Brydone, A.S.; Meek, D.; MacLaine, S. Bone grafting, orthopaedic biomaterials, and the clinical need for bone engineering. *Proc. Inst. Mech. Eng. Part H J. Eng. Med.* **2010**, *224*, 1329–1343.
2. Campana, V.; Milano, G.; Pagano, E.; Barba, M.; Cicione, C.; Salonna, G.; Lattanzi, W.; Logroscino, G. Bone substitutes in orthopaedic surgery: from basic science to clinical practice. *J. Mater. Sci. Mater. Med.* **2014**, *25*, 2445–2461.
3. US Census Bureau Statistical abstracts of the United States: 2012 - Section 1. Population Available online: www.census.gov/library/publications/2011/compendia/statab/131ed/population.html (accessed on Nov 25, 2019).
4. Bhattacharyya, S.; Wang, H.; Ducheyne, P. Polymer-coated mesoporous silica nanoparticles for the controlled release of macromolecules. *Acta Biomater.* **2012**, *8*, 3429–3435.
5. Chen, S.; Shi, X.; Morita, H.; Li, J.; Ogawa, N.; Ikoma, T.; Hayakawa, S.; Shirosaki, Y.; Osaka, A.; Hanagata, N. BMP-2-loaded silica nanotube fibrous meshes for bone generation. *Sci. Technol. Adv. Mater.* **2011**, *12*, 065003.
6. Lo, K.W.; Ulery, B.D.; Ashe, K.M.; Laurencin, C.T. Studies of bone morphogenetic protein-based surgical repair. *Adv. Drug Deliv. Rev.* **2012**, *64*, 1277–1291.
7. Hwang, C.J.; Vaccaro, A.R.; Lawrence, J.P.; Hong, J.; Schellekens, H.; Alaoui-Ismaili, M.H.; Falb, D. Immunogenicity of bone morphogenetic proteins. *J. Neurosurg. Spine SPI* **2009**, *10*, 443–551.
8. Bessa, P.C.; Casal, M.; Reis, R.L. Bone morphogenetic proteins in tissue engineering: the

road from laboratory to clinic , part II (BMP delivery). *J. Tissue Eng. Regen. Med.* **2008**, *2*, 81–96.

9. Kimura, Y.; Ph, D.; Miyazaki, N.; Eng, M.; Hayashi, N.; Eng, M. Controlled Release of Bone Morphogenetic Protein-2 Enhances Recruitment of Osteogenic Progenitor Cells for De Novo Generation of Bone Tissue. *Tissue Eng. Part A* **2010**, *16*, 1263–1270.
10. Yamashita, J.; Furman, B.R.; Rawls, H.R.; Wang, X.; Agrawal, C.M. The use of dynamic mechanical analysis to assess the viscoelastic properties of human cortical bone. *J. Biomed. Mater. Res.* **2001**, *58*, 47–53.
11. Sun, J.; Li, J.; Li, C.; Yu, Y. Role of bone morphogenetic protein-2 in osteogenic differentiation of mesenchymal stem cells. *Mol. Med. Rep.* **2015**, *12*, 4230–4237.
12. Zhang, Y.; Ma, Y.; Yang, M.; Min, S.; Yao, J.; Zhu, L. Expression , purification , and refolding of a recombinant human bone morphogenetic protein 2 in vitro. *Protein Expr. Purif.* **2011**, *75*, 155–160.
13. Jung, H.; Yook, S.; Han, C.; Jang, T.; Kim, H.; Koh, Y.; Estrin, Y. Highly aligned porous Ti scaffold coated with bone morphogenetic protein-loaded silica / chitosan hybrid for enhanced bone regeneration. *J. Biomed. Mater. Res. Part B Appl. Biomater.* **2014**, *102B*, 913–921.
14. Schrier, J.A.; Deluca, P.P. Recombinant Human Bone Morphogenetic Protein-2 Binding and Incorporation in PLGA Microsphere Delivery Systems. *Pharm. Dev. Technol.* **1999**, *4*, 611–621.
15. Johnson, M.R.; Lee, H.; Bellamkonda, R. V; Guldberg, R.E. Sustained release of BMP-2 in a lipid-based microtube vehicle. *Acta Biomater.* **2009**, *5*, 23–28.
16. Li, Y.; Song, Y.; Ma, A.; Li, C. Surface Immobilization of TiO2 Nanotubes with Bone Morphogenetic Protein-2 Synergistically Enhances Initial Preosteoblast Adhesion and

Osseointegration. *Biomed Res. Int.* **2019**, *2019*, 5697250.

17. Vlasenkova, M.I.; Dolinina, E.S.; Parfenyuk, E. V Preparation of mesoporous silica microparticles by sol-gel/emulsion route for protein release. *Pharm. Dev. Technol.* **2018**, *24*, 243–252.

18. Yang, W.; Hellner, B.; Baneyx, F. Self-Immobilization of Car9 Fusion Proteins within High Surface Area Silica Sol-Gels and Dynamic Control of Protein Release. *Bioconjug. Chem.* **2016**, *27*, 2450–2459.

19. Tonon, G.; Morpurgo, M. Sol-gel derived silica polymers for the sustained release of proteins 2008.

20. Chen, Y.C.; Smith, T.; Hicks, R.H.; Doekhie, A.; Koumanov, F.; Wells, S.A.; Edler, K.J.; Van Den Elsen, J.; Holman, G.D.; Marchbank, K.J.; et al. Thermal stability, storage and release of proteins with tailored fit in silica. *Sci. Rep.* **2017**, *7*, 1–8.

21. Chen, Y.-C.; Liu, C.-P.; Yang, C.-K.; Huang, B.-Y.; Liu, C.-Y. Preparation and Release Properties of Sol-Gel Encapsulated Proteins. *J. Anal. Sci. Methods Instrum.* **2013**, *03*, 11–16.

22. Zdarta, J.; Sałek, K.; Kołodziejczak-radzimska, A.; Siwińska-stefańska, K.; Szwarc-rzepka, K.; Norman, M.; Klapiszewski, Ł.; Bartczak, P.; Kaczorek, E.; Jesionowski, T. Immobilization of Amano Lipase A onto Stöber silica surface: process characterization and kinetic studies. *Open Chem.* **2015**, *13*, 138–148.

23. Reiner, T.; Kababya, S.; Gotman, I. Protein incorporation within Ti scaffold for bone ingrowth using Sol-gel SiO2 as a slow release carrier. *J. Mater. Sci. Mater. Med.* **2008**, *19*, 583–589.

24. Ronda, L.; Bruno, S.; Campanini, B.; Mozzarelli, A.; Abbruzzetti, S. Immobilization of Proteins in Silica Gel: Biochemical and Biophysical Properties. *Curr. Org. Chem.* **2015**,

19, 15–18.

25. Brinker, C.J.; Scherer, G.W. *Sol-Gel Science: The Physics and Chemistry of Sol-Gel Processing*; Brinker, C.J., Scherer, G.W., Eds.; Academic Press: San Diego, CA, 1990; ISBN 9780080571034.
26. Lambert, S.; Alié, C.; Pirard, J.P.; Heinrichs, B. Study of textural properties and nucleation phenomenon in Pd/SiO2, Ag/SiO2 and Cu/SiO2 cogelled xerogel catalysts. *J. Non. Cryst. Solids* **2004**, *342*, 70–81.
27. Andreani, T.; Souza, A.L.R. de; Silva, A.M.; Souto, E.B. Sol–Gel Carrier System: A Novel Controlled Drug Delivery. In *Patenting Nanomedicines: Legal Aspects, Intellectual Property and Grant Opportunities*; Souto, E.B., Ed.; Springer-Verlag Berlin Heidelberg: Heidelberg, 2012; pp. 1551–1660 ISBN 978-3-642-29264-4.
28. Jin, W.; Brennan, J.D. Properties and applications of proteins encapsulated within sol-gel derived materials. *Anal. Chim. Acta* **2002**, *461*, 1–36.
29. He, Q.; Shi, J.; Zhu, M.; Chen, Y.; Chen, F. The three-stage in vitro degradation behavior of mesoporous silica in simulated body fluid. *Microporous Mesoporous Mater.* **2010**, *131*, 314–320.
30. Wang, X.; Ahmed, N. Ben; Alvarez, G.S.; Tuttolomondo, M. V; Hélary, C.; Desimone, M.F.; Coradin, T. Sol-Gel Encapsulation of Biomolecules and Cells for Medicinal Applications. *Curr. Top. Med. Chem.* **2015**, *15*, 223–244.
31. Shao, Z.; Cheng, X.; Zheng, Y. Facile co-precursor sol-gel synthesis of a novel amine-modified silica aerogel for high efficiency carbon dioxide capture. *J. Colloid Interface Sci.* **2018**, *530*, 412–423.
32. Anderson, A.M.; Carroll, M.K.; Green, E.C.; Melville, J.T.; Bono, M.S. Hydrophobic silica aerogels prepared via rapid supercritical extraction. *J. Sol-Gel Sci. Technol.* **2010**,

53, 199–207.

33. Santos, E.M.; Radin, S.; Ducheyne, P. Sol-gel derived carrier for the controlled release of proteins. *Biomaterials* **1999**, *20*, 1695–1700.

34. Song, H.K.; Suh, S.W. Kunitz-type Soybean Trypsin Inhibitor Revisited : Refined Structure of its Complex with Porcine Trypsin Reveals an Insight into the Interaction Between a Homologous Inhibitor from Erythrina caffra and Tissue-type Plasminogen Activator. *J. Mol. Biol.* **1998**, *275*, 347–363.

35. Scheufler, C.; Sebald, W.; Hülsmeyer, M. Crystal structure of human bone morphogenetic protein-2 at 2.7 Å resolution1. *J. Mol. Biol.* **1999**, *287*, 103–115.

36. Chang, Y.; Liu, T.C.; Tsai, M. Selective Isolation of Trypsin Inhibitor and Lectin from Soybean Whey by Chitosan / Tripolyphosphate / Genipin Co-Crosslinked Beads. *Int. J. Mol. Sci.* **2014**, *15*, 9979–9990.

37. Yang, J.; Shi, P.; Tu, M.; Wang, Y.; Liu, M.; Fan, F.; Du, M. Bone morphogenetic proteins: Relationship between molecular structure and their osteogenic activity. *Food Sci. Hum. Wellness* **2014**, *3*, 127–135.

38. Hum, J.; Boccaccini, A.R. Bioactive glasses as carriers for bioactive molecules and therapeutic drugs : a review. *J. Mater. Sci. Mater. Med.* **2012**, *23*, 2317–2333.

39. Agrawal, C.M.; Best, J.; Heckman, J.D.; Boyan, B.D. Protein release kinetics of a biodegradable implant for fracture. *Biomaterials* **1995**, *16*, 1255–1260.

40. Tilkin, R.G.; Colle, X.; Argento Finol, A.; Régibeau, N.; Mahy, J.G.; Grandfils, C.; Lambert, S.D. Protein encapsulation in functionalized sol-gel silica : Effect of the encapsulation method on the release kinetics and the activity. *Microporous Mesoporous Mater.* **2020**, *308*, 110502.

41. Chaudhari, A.; Mv, C.; Martens, J.; Vandamme, K.; Naert, I.; Bone, D.J. Bone tissue

response to BMP-2 adsorbed on amorphous microporous silica implants. *J. Clin. Periodontol.* **2012**, *39*, 1206–1213.

42. Chaudhari, A.; Duyck, J.; Braem, A.; Vleugels, J.; Logeart-avramoglou, H.P.D.; Naert, I.; Martens, J.A.; Vandamme, K. Modified Titanium Surface-Mediated Effects on Human Bone Marrow Stromal Cell Response. *Materials (Basel).* **2013**, *2*, 5533–5548.

43. Tang, W.; Lin, D.; Yu, Y.; Niu, H.; Guo, H.; Yuan, Y.; Liu, C. Bioinspired trimodal macro / micro / nano-porous scaffolds loading rhBMP-2 for complete regeneration of critical size bone defect. *Acta Biomater.* **2016**, *32*, 309–323.

44. Gan, Q.; Zhu, J.; Yuan, Y.; Liu, H.; Qian, J.; Li, Y.; Liu, C. A dual-delivery system of pH-responsive chitosan-functionalized mesoporous silica nanoparticles bearing BMP-2 and dexamethasone for enhanced bone regeneration. *J. Mater. Chem. B* **2015**, *3*, 2056–2066.

45. Tan, H.; Yang, S.; Dai, P.; Li, W.; Yue, B. Preparation and physical characterization of calcium sulfate cement / silica-based mesoporous material composites for controlled release of BMP-2. *Int. J. Nanomedicine* **2015**, *10*, 4341–4350.

46. Ehlert, N.; Hoffmann, A.; Luessenhop, T.; Gross, G.; Mueller, P.P.; Stieve, M.; Lenarz, T.; Behrens, P. Amino-modified silica surfaces efficiently immobilize bone morphogenetic protein 2 (BMP2) for medical purposes. *Acta Biomater.* **2011**, *7*, 1772–1779.

47. Li, X.; Lin, W.; Xing, F. The Degradation and BMP release Dynamics of Silica-based Xerogels Modified by adding Calcium and Magnesium or Sintering Process. *Appl. Mech. Mater.* **2012**, *151*, 378–382.

48. Nicoll, S.B.; Radin, S.; Santos, E.M.; Tuan, R.S.; Ducheyne, P. In vitro release kinetics of biologically active transforming growth factor-β1 from a novel porous glass carrier. *Biomaterials* **1997**, *18*, 853–859.

49. Mahy, J.G.; Tasseroul, L.; Zubiaur, A.; Geens, J.; Brisbois, M.; Herlitschke, M.; Hermann,

R.; Heinrichs, B.; Lambert, S.D. Highly dispersed iron xerogel catalysts for p-nitrophenol degradation by photo-Fenton effects. *Microporous Mesoporous Mater.* **2014**, *197*, 164–173.

50. Alié, C.; Ferauche, F.; Pirard, R.; Lecloux, A.J.; Pirard, J.-P. Preparation of low-density xerogels by incorporation of additives during synthesis. *J. Non. Cryst. Solids* **2001**, *289*, 88–96.

51. Lecloux, A. Exploitation des isothermes d'adsorption et de désorption d'azote pour l'étude de la texture des solides poreux. *Mémoires Société des Sci. Liege* **1971**, *4*, 169–209.

52. Lecloux, A. Texture of Catalysts. In *Catalysis: Science and Technology, vol. 2*; Anderson, J.R., Boudart, M., Eds.; Berlin, 1981; p. 171 ISBN 978-3-642-93249-6.

53. Park, J.; Regalbuto, J.R. A Simple, Accurate Determination of Oxide PZC and the Strong Buffering Effect of Oxide Surfaces at Incipient Wetness. *J. Colloid Interface Sci.* **1995**, *175*, 239–252.

54. Lambert, S.; Job, N.; Souza, L.D.; Fernando, M.; Pereira, R.; Pirard, R.; Heinrichs, B.; Luis, J.; Pirard, J.; Regalbuto, J.R. Synthesis of very highly dispersed platinum catalysts supported on carbon xerogels by the strong electrostatic adsorption method. *J. Catal.* **2009**, *261*, 23–33.

55. Alié, C. Synthesis of silica with tailored morphology by sol-gel process, Université de Liège, 2001.

56. Mansur, H.; Oréfice, R.; Pereira, M.; Lobato, Z. FTIR and UV-vis study of chemically engineered biomaterial surfaces for protein immobilization. *Spectroscopy* **2002**, *16*, 351–360.

57. Péré, E.; Cardy, H.; Cairon, O.; Simon, M.; Lacombe, S. Quantitative assessment of organic compounds adsorbed on silica gel by FTIR and UV-VIS spectroscopies: the

contribution of diffuse reflectance spectroscopy. *Vib. Spectrosc.* **2001**, *25*, 163–175.

58. Antony, R.; Theodore David Manickam, S.; Kollu, P.; Chandrasekar, P.V.; Karruppasamy, K.; Balakumar, S. Highly dispersed Cu(II), Co(II) and Ni(II) catalysts covalently immobilized on imine-modified silica for cyclohexane oxidation with hydrogen peroxide. *RSC Adv.* **2014**, *4*, 24820–24830.

59. Capeletti, L.B.; Baibich, I.M.; Butler, I.S.; dos Santos, J.H.Z. Infrared and Raman spectroscopic characterization of some organic substituted hybrid silicas. *Spectrochim. Acta Part A Mol. Biomol. Spectrosc.* **2014**, *133*, 619–625.

60. Osswald, J.; Fehr, K.T. FTIR spectroscopic study on liquid silica solutions and nanoscale particle size determination. *J. Mater. Sci.* **2006**, *41*, 1335–1339.

61. Warring, S.L.; Beattie, D.A.; Mcquillan, A.J. Sur fi cial Siloxane-to-Silanol Interconversion during Room- Temperature Hydration/Dehydration of Amorphous Silica Films Observed by ATR-IR and TIR-Raman Spectroscopy. *Langmuir* **2016**, *32*, 1568–1576.

62. Etienne, M.; Walcarius, A. Analytical investigation of the chemical reactivity and stability of aminopropyl-grafted silica in aqueous medium. *Talanta* **2003**, *59*, 1173–1188.

63. Adumeau, L.; Genevois, C.; Roudier, L.; Schatz, C.; Adumeau, L.; Genevois, C.; Roudier, L.; Schatz, C.; Couillaud, F. Impact of surface grafting density of PEG macromolecules on dually fluorescent silica nanoparticles used for the in vivo imaging of subcutaneous tumors. *Biochim. Biophys. Acta* **2017**, *1861*, 1587–1596.

64. Bharathi, S.; Fishelson, N.; Lev, O. Direct Synthesis and Characterization of Gold and Other Noble Metal Nanodispersions in Sol - Gel-Derived Organically Modified Silicates. *Langmuir* **1999**, *15*, 1929–1937.

65. Mohan, S.; Sundaraganesan, N.; Mink, J. FTIR and Raman studies on benzimidazole.

Spectrochim. Acta **1991**, *47A*, 1111–1115.

66. Mary, Y.S.; Jojo, P.. J.; Panicker, C.Y.; Alsenoy, C. Van; Ataei, S.; Yildiz, I. Quantum mechanical and spectroscopic (FT-IR , FT-Raman , 1H NMR and UV) investigations of 2-(phenoxymethyl) benzimidazole. *Spectrochim. Acta Part A Mol. Biomol. Spectrosc.* **2014**, *125*, 12–24.

67. Coates, J. Interpretation of Infrared Spectra , A Practical Approach. In *Encyclopedia of Analytical Chemistry*; Meyers, R.A., Ed.; John Wiley & Sons Ltd: Chichester, 2000; pp. 10815–10837 ISBN 9780470027318.

68. Célino, A.; Gonc, O.; Jacquemin, F.; Fréour, S. Qualitative and quantitative assessment of water sorption in natural fibres using ATR-FTIR spectroscopy. *Carbohydr. Polym.* **2014**, *101*, 163–170.

69. Zhuravlev, L.T. Concentration of Hydroxyl Groups on the Surface of Amorphous Silicas. *Langmuir* **1987**, *3*, 316–318.

70. Thommes, M.; Kaneko, K.; Neimark, A. V; Olivier, J.P.; Rodriguez-Reinoso, F.; Rouquerol, J.; Sing, K.S.W. Physisorption of gases, with special reference to the evaluation of surface area and pore size distribution (IUPAC Technical Report). *Pure Appl. Chem.* **2015**, *87*, 1051–1069.

71. Mahy, J.G.; Tasseroul, L.; Herlitschke, M.; Hermann, R.P.; Lambert, S.D. Fe 3 + / iron oxide / SiO 2 xerogel catalysts for p -nitrophenol degradation by photo-Fenton effects : Influence of thermal treatment on catalysts texture. *Mater. Today Proc.* **2016**, *3*, 464–469.

72. Lambert, S.; Sacco, L.; Ferauche, F.; Heinrichs, B.; Noels, A.; Pirard, J. Synthesis of SiO2 xerogels and Pd/SiO2 cogelled xerogel catalysts from silylated acetylacetonate ligand. *J. Non. Cryst. Solids* **2004**, *343*, 109–120.

73. Kosmulski, M. Compilation of PZC and IEP of sparingly soluble metal oxides and

hydroxides from literature. *Adv. Colloid Interface Sci.* **2009**, *152*, 14–25.

74. Hou, C.; Gheczy, N.; Messmer, D.; Szyman, K.; Adamcik, J.; Jarzebski, A.B.; Walde, P. Stable Immobilization of Enzymes in a Macro- and Mesoporous Silica Monolith. *ACS Omega* **2019**, *4*, 7795–7806.

75. Gustafsson, H.; Thörn, C.; Holmberg, K. A comparison of lipase and trypsin encapsulated in mesoporous materials with varying pore sizes and pH conditions. *Colloids Surfaces B Biointerfaces* **2011**, *87*, 464–471.

76. Jeyachandran, Y.L.; Mielczarski, J.A.; Mielczarski, E.; Rai, B. Efficiency of blocking of non-specific interaction of different proteins by BSA adsorbed on hydrophobic and hydrophilic surfaces. *J. Colloid Interface Sci.* **2010**, *341*, 136–142.

77. Tanaka, M.; Motomura, T.; Kawada, M.; Anzai, T.; Kasori, Y.; Shiroya, T.; Shimura, K.; Onishi, M.; Mochizuki, A. Blood compatible aspects of poly (2-methoxyethylacrylate) (PMEA) - relationship between protein adsorption and platelet adhesion on PMEA surface. *Biomaterials* **2000**, *21*, 1471–1481.

78. Cassano, D.; Mapanao, A.-K.; Summa, M.; Vlamidis, Y.; Giannone, G.; Santi, M.; Guzzolino, E.; Pitto, L.; Poliseno, L.; Bertorelli, R.; et al. Biosafety and Biokinetics of Noble Metals: The Impact of Their Chemical Nature. *ACS Appl. Biomater.* **2019**, *2*, 4464–4470.

79. Cassano, D.; Martir, D.R.; Signore, G.; Piazzaa, V.; Voliani, V. Biodegradable hollow silica nanospheres containing gold nanoparticle arrays. *Chem. Commun.* **2015**, *51*, 9939–9942.